Cell Research (2017) :1157-1177.
© 2017 IBCB, SIBS, CAS All rights reserved 1001-0602/17 $ 32.00
www.nature.com/cr

ORIGINAL ARTICLE

Fibroblasts in an endocardial fibroelastosis disease model mainly originate from mesenchymal derivatives of epicardium

Hui Zhang[1, 2, 3, *], Xiuzhen Huang[1, 2, *], Kuo Liu[1, 2, 3, *], Juan Tang[1, 2, *], Lingjuan He[1, 2], Wenjuan Pu[1, 2], Qiaozhen Liu[1, 2], Yan Li[1, 2], Xueying Tian[1, 2], Yue Wang[1, 2], Libo Zhang[1, 2], Ying Yu[2], Hongyan Wang[1], Ronggui Hu[1], Fengchao Wang[4], Ting Chen[4], Qing-Dong Wang[5], Zengyong Qiao[6], Li Zhang[7], Kathy O Lui[8], Bin Zhou[1, 2, 3, 9]

[1]The State Key Laboratory of Cell Biology, CAS Center for Excellence in Molecular Cell Science, Shanghai Institute of Biochemistry and Cell Biology, Chinese Academy of Sciences, University of Chinese Academy of Sciences, Shanghai 200031, China; [2]Key Laboratory of Nutrition and Metabolism, Institute for Nutritional Sciences, Shanghai Institutes for Biological Sciences, Graduate School of the Chinese Academy of Sciences, Chinese Academy of Sciences, Shanghai 200031, China; [3]School of Life Science and Technology, ShanghaiTech University, Shanghai 201210, China; [4]National Institute of Biological Sciences, Beijing 102206, China; [5]Cardiovascular and Metabolic Diseases, Innovative Medicines and Early Clinical Development Biotech Unit, AstraZeneca, Mölndal 43183, Sweden; [6]Department of Cardiovascular Medicine, Southern Medical University Affiliated Fengxian Hospital, Shanghai 201499, China; [7]Department of Cardiology, the First Affiliated Hospital, School of Medicine, Zhejiang University, 79 Qingchun Road, Hangzhou, Zhejiang 310003, China; [8]Department of Chemical Pathology, Li Ka Shing Institute of Health Sciences, The Chinese University of Hong Kong, Prince of Wales Hospital, Shatin, Hong Kong SAR 999077, China; [9]Key Laboratory of Regenerative Medicine of Ministry of Education, Institute of Aging and Regenerative Medicine, Jinan University, Guangzhou, Guangdong 510632, China

Endocardial fibroelastosis (EFE) refers to the thickening of the ventricular endocardium as a result of *de novo* deposition of subendocardial fibrous tissue layers during neonatal heart development. The origin of EFE fibroblasts is proposed to be postnatal endocardial cells that undergo an aberrant endothelial-to-mesenchymal transition (EndMT). Genetic lineage tracing of endocardial cells with the inducible endocardial Cre line *Npr3-CreER* and the endothelial cell tracing line *Cdh5-CreER* on an EFE-like model did not reveal any contribution of neonatal endocardial cells to fibroblasts in the EFE-like tissues. Instead, lineage tracing of embryonic epicardium by *Wt1-CreER* suggested that epicardium-derived mesenchymal cells (MCs) served as the major source of EFE fibroblasts. By labeling MCs using *Sox9-CreER*, we confirmed that MCs of the embryonic heart expand and contribute to the majority of neonatal EFE fibroblasts. During this pathological process, TGFβ signaling, the key mediator of fibroblasts activation, was highly upregulated in the EFE-like tissues. Targeting TGFβ signaling by administration of its antagonist bone morphogenetic protein 7 effectively reduced fibroblast accumulation and tissue fibrosis in the EFE-like model. Our study provides genetic evidence that excessive fibroblasts in the EFE-like tissues mainly originate from the epicardium-derived MCs through epicardial to mesenchymal transition (EpiMT). These EpiMT-derived fibroblasts within the EFE-like tissues could serve as a potential therapeutic target.

***Keywords*:** lineage tracing; heart disease; fibrosis; endocardium; epicardium

Cell Research (2017) **27**:1157-1177. doi:10.1038/cr.2017.103; published online 15 August 2017

Introduction

Endocardial fibroelastosis (EFE) refers to the pathological condition that often causes sudden death in infants and children [1-4]. EFE is characterized by diffuse profound thickening of the endocardium with abnormal deposition of collagen and elastin predominantly in the left ventricle [2, 3, 5-8]. The accumulated collagen and elastin form a *de novo* subendocardial fibrous tissue layer,

*These four authors contributed equally to this work.
Correspondence: Hui Zhang[a], Bin Zhou[b]
[a]E-mail: zhanghui1@shanghaitech.edu.cn
[b]E-mail: zhoubin@sibs.ac.cn
Received 19 March 2017; revised 18 June 2017; accepted 29 June 2017; published online 15 August 2017

which encapsulates the underlying myocardium. It is thought that EFE limits ventricular diastolic compliance and restricts ventricular growth [9, 10]. EFE is correlated to a variety of diseases such as hypoplastic left heart syndrome (HLHS) and bacterial myocarditis. It has been reported that fetal intervention and postnatal surgical removal of EFE tissues could renew left ventricular growth and restore biventricular physiology in some cases of HLHS [11, 12]. Nevertheless, effective measures are still needed to inhibit formation of EFE tissues. Therefore, understanding the pathophysiological progression of EFE would help provide new insights into the search for the potential therapeutic targets in treatment of EFE.

The main cellular population of EFE tissues is fibroblasts that generates extracellular matrix. Excessive deposition of fibroblasts and extracellular matrix leads to development of fibrosis, which is one of the main pathological features of EFE. To date, little is known about the cellular origins of EFE. It would therefore be helpful to unravel the cellular origins of EFE fibroblasts in order to delineate the pathogenesis of EFE and thereby design potential therapeutic strategies. As its name suggests, EFE is largely restricted to the endocardial tissue. It has been reported that the origin of EFE fibroblasts lies in the endocardial to mesenchymal transition [13]. Moreover, the ability to surgically remove the thickened fibroelastic layer without myocardial contamination suggests, but does not prove, that the fibrotic tissue might be derived from endocardium [12].

During murine heart development, at approximately embryonic day (E)12.5, epicardial cells migrate into the myocardium and give rise to mesenchymal cells (MCs) via the epithelial-to-mesenchymal transition (EpiMT). These epicardial-derived mesenchymal cells (Epi-MCs) then contribute to several lineages of the heart, including fibroblasts, pericytes and smooth muscle cells (SMCs) [14-18]. In addition, at E9.5, endocardial cells undergo endothelial-to-mesenchymal transition (EndMT) and populate the endocardial cushions with MCs. Recent studies have suggested that these endocardial-derived mesenchymal cells (Endo-MCs) could migrate into the myocardium and differentiate into fibroblasts, pericytes and SMCs [19-21]. These studies suggest that both Epi-MCs and Endo-MCs could contribute to cardiac fibroblasts during heart development. In normal adult hearts, lineage tracing experiments with the *Wt1-Cre* line has shown that over 90% fibroblasts in the ventricular walls and 30% fibroblasts in the ventricular septum are derived from the embryonic epicardium [19]. Moreover, fate mapping of endothelium using the *Tie2-Cre* and *Ve-cadherin* (*Cdh5*)-*CreER* lines has demonstrated a contribution of embryonic endocardial-derived fibroblasts complementary to those of the epicardium. Embryonic endocardium contributes about 12% fibroblasts in the left ventricular walls and 64% fibroblasts in the ventricular septum [19]. Therefore, fibroblasts of normal adult hearts are mainly derived from the embryonic Epi-MCs with a minor contribution from the embryonic Endo-MCs [19].

Following cardiac injury, it has been reported that the endothelium and hematopoietic cells are origins of cardiac fibroblasts in various fibrosis models including ascending aorta constriction, chronic allograft rejection, myocardial infarction, diabetes and the angiotensin-induced cardiac fibrosis model [22-26]. Notably, inhibition of EndMT during fibrosis reduces fibroblast deposition and facilitates heart repair [22]. Fibrotic EndMT and circulating fibroblast progenitors represent two potential therapeutic targets for fibrosis [27]. However, recent studies argued that new fibroblasts in injured heart are mainly derived from resident fibroblasts, which originate from embryonic Epi-MCs and Endo-MCs [19, 21]. Lineage tracing studies for adult endothelium (*Ve-cadherin-CreER*), adult epicardium (*Wt1-CreER* and *Tbx18-CreER*) or hematopoietic cells (*Vav-Cre*) have not provided convincing evidence for their contribution to fibroblasts following myocardial stress [19]. Moreover, neither transplantation studies nor parabiosis experiments support the notion that new cardiac fibroblasts are derived from bone marrow or circulating cells [21].

EFE is a specialized form of fibrosis that involves excessive fibroblast deposition in the thickened endocardial layer. Here, by virtue of multiple independent Cre knock-in mouse lines, we confirmed that postnatal endothelium, including both endocardium and coronary endothelium, did not contribute to fibrotic fibroblasts in mouse EFE-like models. Instead, embryonic MCs labeled by *Sox9-CreER* gave rise to the majority of EFE fibroblasts. Specifically, Epi-MCs but not Endo-MCs were the major sources of fibroblasts within the EFE-like tissues. We also detected high expression of TGFβ in the EFE-like tissues, and treatment of mice with bone morphogenetic protein 7 (BMP7), an antagonist for TGFβ signaling, effectively reduces fibroblast accumulation and tissue fibrosis. Our results suggest that therapeutic strategies in reducing pathogenic EFE fibroblasts should shift from the focus of targeting the postnatal EndMT-derived fibroblasts to pathways regulating development of the embryonic EpiMT-derived fibroblasts.

Results

Mouse EFE-like model of unloaded heterotopically transplanted hearts

The pathogenesis of human EFE remains obscure. It

often occurs in fetal or neonatal hearts with hypoplastic left heart syndrome (HLHS), which may result from aortic stenosis and left ventricular dysfunction. From clinical observations, the presence of EFE has a strong relationship with the decreased left ventricular blood flow. To mimic the conditions of human fetal/neonatal hearts with EFE, an EFE-like model with a nonworking hemodynamically unloaded heart has been introduced to study EFE for years [13, 28]. In this established model, reduced ventricular and intracavitary blood flow are found, recapitulating the conditions in human fetal hearts with HLHS when the aortic valve closes. Moreover, fibrosis in the EFE-like model may result from ischemia due to reduced blood flow in the hemodynamically unloaded heart.

To investigate the origin of fibroblasts within EFE-like tissues, we first developed the EFE-like mouse model, in which neonatal hearts were heterotopically transplanted into the abdomen of adult mice, as previously described [28, 29]. Such surgery procedures on immature donor hearts could model the pathogenesis of human EFE, which is associated with reduced blood flow at the neonatal stage. Briefly, postnatal day (P)7 mouse heart was collected and implanted as a heterotopic infra-renal graft, where the ascending aorta was surgically linked to the infra-renal aorta and the pulmonary artery was linked to the inferior vena cava anastomoses [28, 29]. The donor hearts were then analyzed at day 12 following transplantation (Figure 1A and 1B). Human EFE has the gross appearance of subendocardial fibrosis; thus we examined the morphology and degree of fibrosis of the heterotopic EFE-like heart transplants by H&E staining, sirius red staining and Collagen staining, respectively. Compared with the native hearts, excessive extracellular matrix was deposited in the subendocardial layers of left ventricles of the heterotopic heart transplants (Figure 1C and Supplementary information, Figure S1A-S1D). To confirm fibrous tissue deposition in the subendocardial layers of the heterotopic heart transplants, we stained heart sections for the fibroblast marker platelet-derived growth factor receptor alpha (PDGFRa); and found that deposition of $PDGFRa^+$ fibroblasts was significantly increased in heterotopic heart transplants (Supplementary information, Figure S1E). We also stained heart sections for an additional, widely used yet less specific fibroblast marker fibroblast-specific protein-1 (FSP1) [13], which also labels some endothelial cells and leukocytes [30]. Similarly, we observed a significant increase in $FSP1^+$ cells in the heterotopic heart transplants compared with the native hearts (Supplementary information, Figure S1F). Taken together, our results showed a successful mouse model recapitulating pathogenesis of EFE via heterotopic heart transplantation.

Lineage tracing of postnatal endothelium shows no evidence for EndMT in EFE-like tissues

Endothelial cells in the heart include both the endocardial and coronary endothelial cells. We generated the *Npr3-CreER* mouse line that specifically marked the endocardium at embryonic stages [31, 32]. To test if *Npr3-CreER* labels postnatal endocardial endothelial cells, we crossed *Npr3-CreER* with the reporter line *Rosa26-loxp-stop-loxp-tdTomato* (*R26-tdTomato*) [33] and treated *Npr3-CreER;R26-tdTomato* pups at postnatal day (P) 5 with tamoxifen. The hearts were then collected at 48 h post treatment. Immunostaining for the tracing reporter tdTomato and the coronary endothelial marker FABP4 on heart sections showed that *Npr3-CreER* labeled endocardial cells but not coronary endothelial cells (Supplementary information, Figure S2A). In addition to the endocardium, we found that *Npr3-CreER* also labeled a subset of epicardial cells (Supplementary information, Figure S2B).

A previous study suggests that fibroblasts in the EFE-like tissues are mainly derived from aberrant EndMT [13]. To verify if the endocardium contributes to fibroblasts within EFE-like tissues, we administered a neonatal *Npr3-CreER;R26-tdTomato* mouse with tamoxifen at P5, and implanted the P7 heart into the abdomen of an adult wild-type mouse. At day 12 following implantation, the donor heart was harvested and analyzed (Figure 1D). Immunostaining for tdTomato, fibroblast marker PDGFRa and endothelial cell-specific marker CDH5 showed that *Npr3-CreER*-labeled endocardial cells did not contribute to any fibroblast within the EFE-like tissues (Figure 1E). Immunostaining for tdTomato, CDH5 and an additional fibroblast marker, FSP1, confirmed that endocardial cells did not contribute to any $FSP1^+CDH5^-$ fibroblast in the EFE-like tissues (Figure 1F). We also traced the neonatal endocardium in native *Npr3-CreER;R26-tdTomato* hearts following tamoxifen induction at P5 and heart collection at P19. In normal hearts, *Npr3-CreER* labeled both endocardial and epicardial cells at P19, but not vascular endothelial cells (Supplementary information, Figure S2C and S2D). In P19 mouse hearts, neither $PDGFRa^+$ nor $FSP1^+$ cells were derived from endocardial cells (Supplementary information, Figure S2E and S2F). Collectively, these data demonstrated that neonatal endocardial cells did not contribute to fibroblasts in either EFE-like or normal hearts (Figure 1G). These data also proved that *Npr3-CreER*-labeled neonatal epicardium did not contribute to fibroblasts in either EFE-like or normal hearts.

We next asked if vascular endothelial cells contribute to new fibroblasts through EndMT [22]. To this end, we

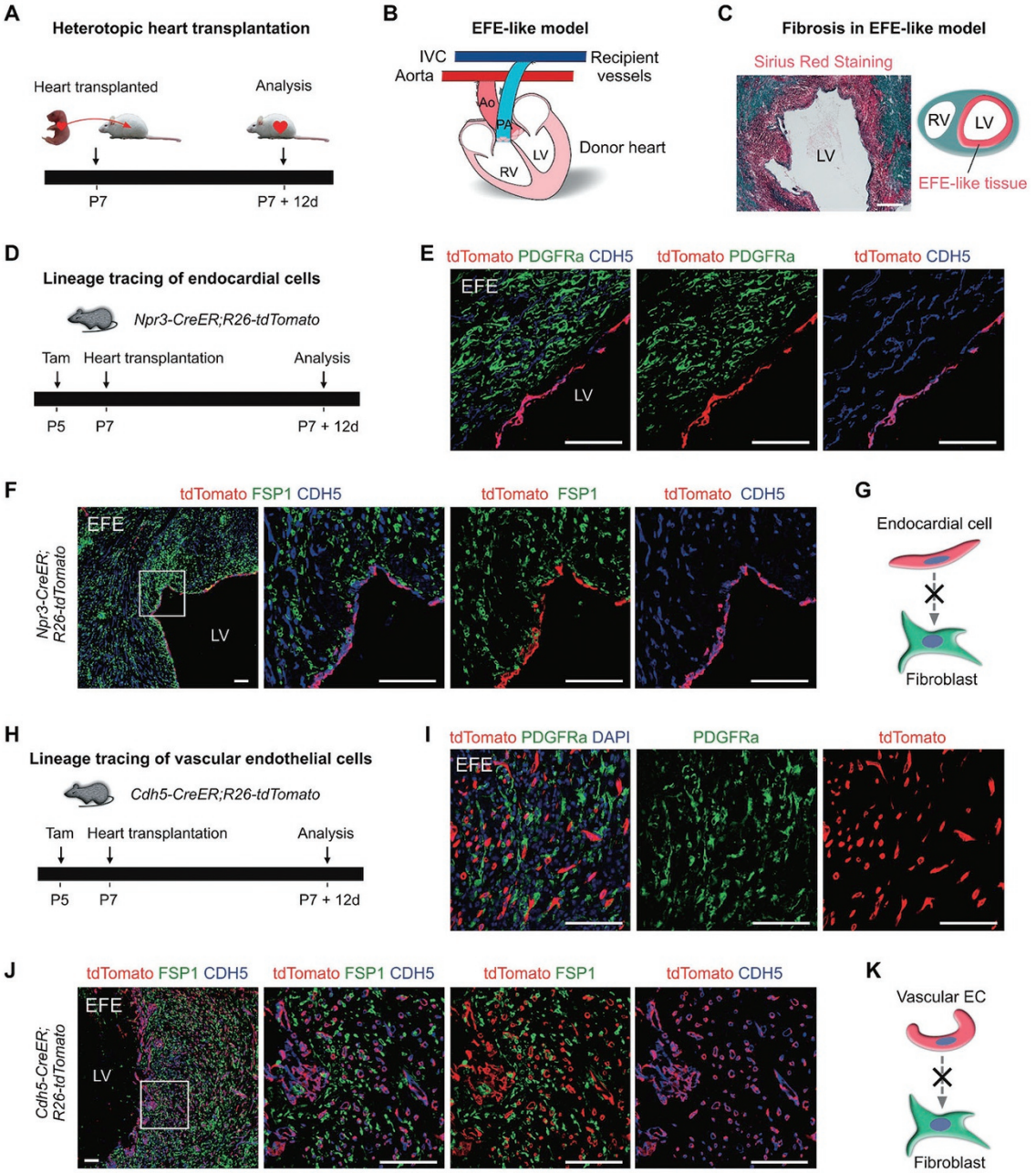

Figure 1 Postnatal endocardial and vascular endothelial cells do not contribute to fibroblasts in the EFE-like tissues. **(A)** Schematic showing experimental strategy. Donor heart from postnatal day (P)7 mouse was implanted into the peritoneal cavity of 8-week-old mouse. Donor hearts were analyzed at day 12 following transplantation. **(B)** Cartoon showing the heterotopic heart transplant model. The ascending aorta was anastomosed to the infrarenal aorta (Ao), and the pulmonary artery (PA) was anastomosed to the infrarenal vena cava (IVC). **(C)** Sirius red staining on heart sections shows EFE-like tissues within the inner layer of LV. **(D)** Schematic figure showing the experimental strategy for lineage tracing of endocardial cells using *Npr3-CreER;R26-tdTomato* mice. Tamoxifen was administered 2 days before heart transplantation. **(E)** Immunostaining for tdTomato, PDGFRa and CDH5 on donor heart sections. **(F)** Immunostaining for tdTomato, FSP1 and CDH5 on donor heart sections shows that endocardial cells do not contribute to $FSP1^{+}CDH5^{-}$ fibroblasts in the EFE-like tissues. Boxed regions are magnified in the right panels. **(G)** Cartoon showing no lineage conversion from endocardial cells to fibroblasts. **(H)** Schematic showing the experimental strategy for lineage tracing of vascular endothelial cells using *Cdh5-CreER;R26-tdTomato* mice. **(I)** Immunostaining for tdTomato and PDGFRa on donor heart sections. **(J)** Immunostaining for tdTomato, FSP1 and CDH5 on donor heart sections shows that vascular endothelial cells (ECs) do not contribute to $FSP1^{+}CDH5^{-}$ fibroblasts in the EFE-like tissues. Boxed regions are magnified in the right panels. **(K)** Cartoon showing no lineage conversion from vascular ECs to fibroblasts. Scale bars, 400 μm in **C**; 100 μm in **E**, **F**, **I**, **J**. LV, left ventricle; RV, right ventricle.

employed *Cdh5-CreER;R26-tdTomato* to address vascular EndMT in EFE-like tissues, as it has been shown that *Cdh5-CreER* labels most coronary vascular endothelial cells [34]. Tamoxifen was administered 2 days before the *Cdh5-CreER;R26-tdTomato* heart was transplanted to the recipient mouse. The donor heart was harvested and analyzed at day 12 following transplantation (Figure 1H). Immunostaining for tdTomato and PDGFRa or FSP1 showed that *Cdh5-CreER*-labeled endothelial cells did not contribute to $PDGFRa^+$ or $FSP1^+CDH5^-$ cells (Figure 1I and 1J). Taken together, our lineage tracing data from *Npr3-CreER* and *Cdh5-CreER* lines demonstrated that endocardial and vascular endothelial cells did not contribute to fibroblasts within the EFE-like tissues (Figure 1G and 1K), suggesting that EndMT is unlikely to be the major mechanism for development of EFE fibroblasts.

Embryonic cardiac MCs are the major source of EFE fibroblasts

Given that some studies have demonstrated that fibroblasts deposited following aortic banding are derived solely from resident fibroblasts, which originate from embryonic Epi-MCs and embryonic Endo-MCs [19, 21], we hypothesized that the fibroblasts within EFE-like tissues were derived from preexisting cardiac MCs within the myocardium before birth. It has been reported that the transcription factor SRY-type box (Sox) 9, which plays critical roles in cardiac valve formation and epicardial migration at embryonic stages, is highly expressed in epicardial cells, Epi-MCs and Endo-MCs [35-37]. Thus we employed the *Sox9-CreER* mouse line to investigate if cardiac MCs contribute to EFE fibroblasts.

We first collected *Sox9-CreER* embryos from E9.5 to E11.5 and examined the expression of the estrogen receptor (ESR), which served as a surrogate for Sox9 expression. Immunostaining for ESR and CDH5 on E9.5 *Sox9-CreER* embryonic sections indicated that expression of ESR/Sox9 was mainly restricted to mesenchymal cells in the atrioventricular canal cushion, a subset of proepicardial cells and epicardial cells, but not in endocardial cells of the ventricular walls (Figure 2A and 2B). Co-staining for ESR and the (pro)epicardial marker TBX18 confirmed expression of ESR/Sox9 by proepicardial cells and epicardial cells (Figure 2A and 2C). At E10.5 and E11.5, immunostaining for ESR and CDH5 or TBX18 revealed similar ESR expression patterns compared to E9.5. Expression of ESR was detected in mesenchymal cells of the atrioventricular canal cushion and epicardial cells, but not in endocardial cells of the ventricular walls (Figure 2A and Supplementary information, Figure S3A-S3D). To further confirm that Sox9 was expressed in EndMT-derived cushion MCs, we collected embryos of *Npr3-CreER;R26-tdTomato* at E10.5, which had been treated with tamoxifen at E8.5, and stained for tdTomato, Sox9 and CDH5. The immunostaining data showed co-localization of Sox9 and tdTomato in the atrioventricular cushion (Supplementary information, Figure S3E), indicating that Sox9 was expressed in endocardial-derived MCs.

Having validated expression of CreER/Sox9 in the early embryonic heart, we utilized *Sox9-CreER* for genetic lineage tracing of MCs in the EFE-like model. We crossed the *Sox9-CreER* mouse strain with the reporter line *R26-tdTomato* to examine the labeling efficiency of MCs by *Sox9-CreER*. Tamoxifen was administered at E9.5 and hearts were harvested at E14.5 (Figure 2D). Immunostaining for tdTomato and the endothelial maker PECAM on E14.5 heart sections showed that tdTomato was robustly detected in the endocardial cushion, epicardium and subepicardial regions (Supplementary information, Figure S4B). Some of these $tdTomato^+$ cells were located in close proximity to $PECAM^+$ endothelial cells, but they were rarely endothelial cells (0.63% ± 0.23%, $n = 4$; Supplementary information, Figure S4B). Instead, immunostaining for the epicardial marker TBX18 showed that a high percentage of epicardial cells were $tdTomato^+$ cells (95.42% ± 1.51%, $n = 4$; Supplementary information, Figure S4C). We also performed co-staining for tdTomato and the embryonic cardiac mesenchymal cell markers PDGFRa or platelet derived growth factor receptor beta (PDGFRb); and found that *Sox9-CreER* efficiently labeled cushion MCs and epicardial-derived MCs (Figure 2E and 2F). Taken together, *Sox9-CreER* labeled cardiac MCs that included both Endo-MCs and Epi-MCs at early-to-mid embryonic stages.

We next followed the cell fate of *Sox9-CreER*-labeled cardiac MCs to the postnatal stage (Figure 3A). We collected normal hearts at P19 and stained heart sections for PDGFRa, PDGFRb and alpha smooth muscle actin (aSMA), which are markers for fibroblasts, pericytes and SMCs, respectively, at this stage. We found that $tdTomato^+$ cells constituted 91.18% ± 1.32% of $PDGFRa^+$ fibroblasts, 93.60% ± 1.39% of $PDGFRb^+$ pericytes, and 96.86% ± 1.74% of $aSMA^+$ SMCs ($n = 4$; Figure 3B-3E). These data suggested that *Sox9-CreER*-labeled cardiac MCs contributed to the majority of fibroblasts, pericytes and SMCs in normal heart during postnatal homeostasis.

As hematopoietic cells have been reported as potential origins of fibroblasts [23, 24, 26], we therefore examined whether *Sox9-CreER* labels resident myeloid cells or circulating hematopoietic cells. First we collected P7 hearts from *Sox9-CreER;R26-tdTomato* mice, which were administered with tamoxifen at E9.5. Immunostaining for tdTomato along with hematopoietic marker CD45 or macrophage marker F4/80 and CD11b suggested that

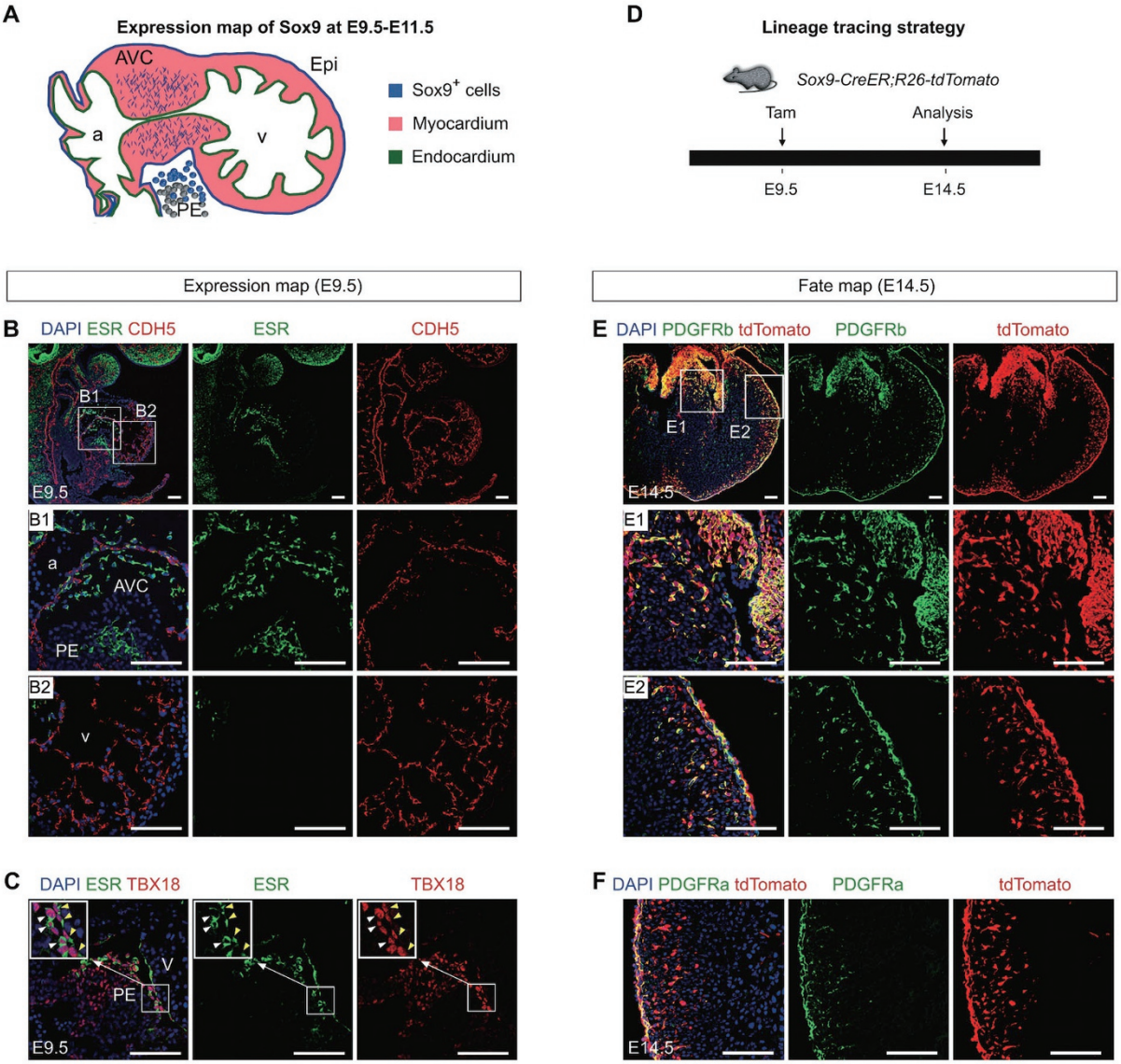

Figure 2 Sox9 labels mesenchymal cells at early embryonic stages. **(A)** Cartoon showing the expression map of Sox9 at E9.5 to E11.5. Blue coloring indicates Sox9$^+$ cells including endocardial cushion mesenchymal cells, proepicardial and epicardial cells. **(B)** Immunostaining for CDH5 and ESR, where ESR is a surrogate of Sox9, on E9.5 *Sox9-CreER* embryonic sections shows that ESR/Sox9 is expressed in cushion mesenchymal cells and proepicardial cells, but not in ventricular endocardial cells at E9.5. B1 and B2 are magnified images of boxed regions in **B**. **(C)** Immunostaining for ESR and TBX18 shows that ESR is detected in proepicardial cells and epicardial cells at E9.5. White arrowheads indicate ESR$^+$ proepicardial cell and yellow arrowheads indicate ESR$^+$ epicardial cells. **(D)** Lineage tracing strategy using *Sox9-CreER*;*R26-tdTomato* embryos. Tamoxifen was administered at E9.5 and embryos were collected for analysis at E14.5. **(E)** Immunostaining for tdTomato and PDGFRb on heart sections of E14.5 *Sox9-CreER*;*R26-tdTomato* embryos. E1 and E2 are magnified images of boxed regions in **E**. **(F)** Immunostaining for tdTomato and PDGFRa on heart sections of *Sox9-CreER*;*R26-tdTomato* mice at E14.5 confirms that tdTomato labels epicardial-derived mesenchymal cells. a, atrium; AVC, atrioventricular canal; Epi, epicardium; PE, proepicardium; v, ventricle. Scale bar, 100 μm.

Sox9-CreER did not label resident myeloid cells in hearts (Supplementary information, Figure S5A-S5C). Next, we collected the blood cells of *Sox9-CreER;R26-tdTomato* mice, and found that there were very few tdTomato$^+$ hematopoietic cells (Supplementary information, Figure S5D-S5E). Collectively, *Sox9-CreER* rarely labeled hematopoietic cells.

To determine the contribution of cardiac MCs to

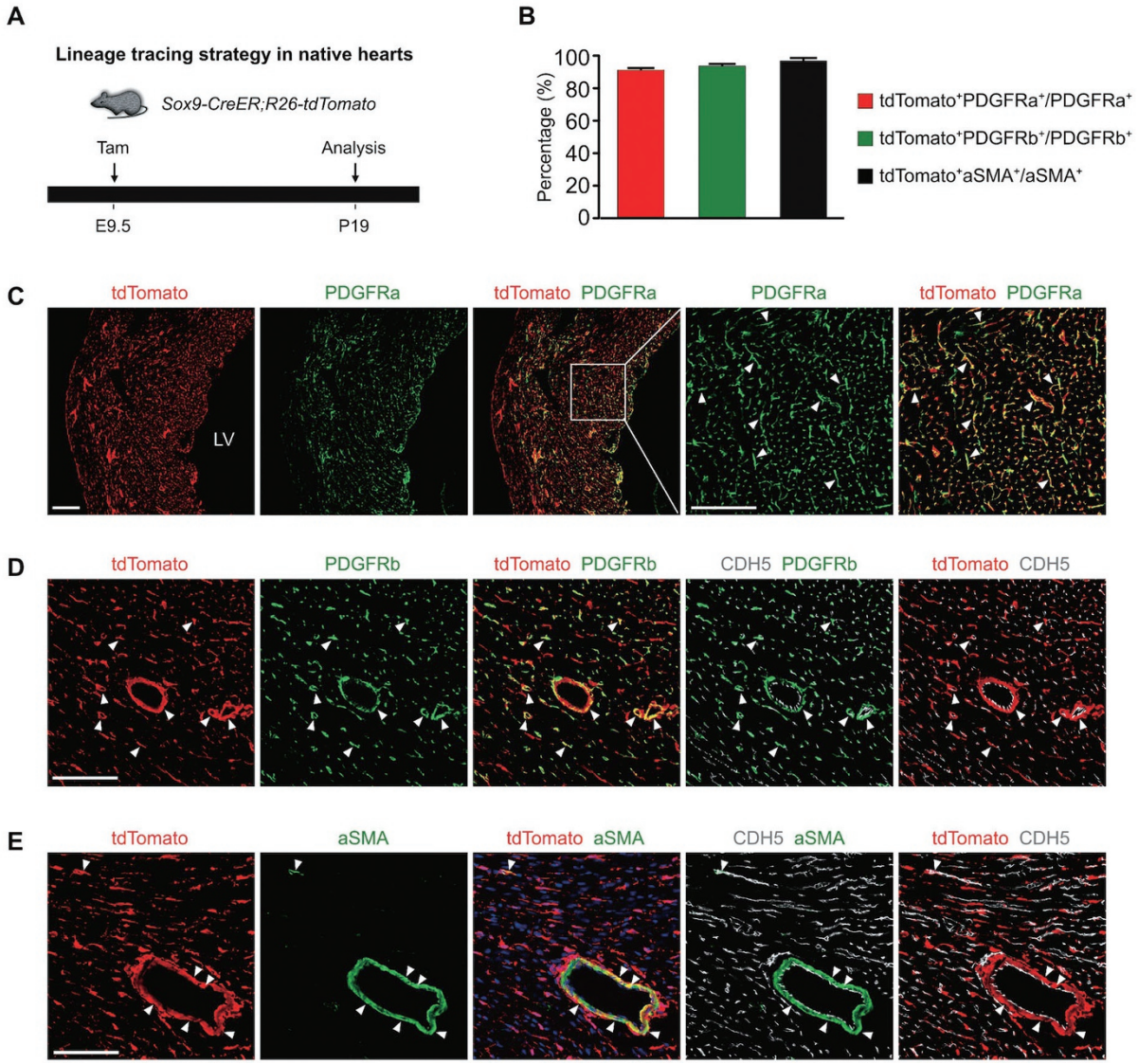

Figure 3 *Sox9-CreER* labeled embryonic mesenchymal cells contribute to fibroblasts, pericytes and smooth muscle cells in the native hearts. **(A)** Schematic showing the strategy for lineage tracing of Sox9$^+$ cells using *Sox9-CreER*;*R26-tdTomato* mice. **(B)** Quantification of the percentage of labeled cells by *Sox9-CreER* at P19. n = 4. **(C)** Immunostaining for tdTomato and fibroblast marker PDGFRa shows that *Sox9-CreER* labels most PDGFRa$^+$ fibroblasts at P19. Arrowheads indicate td-Tomato$^+$PDGFRa$^+$ fibroblasts. Boxed region is magnified in the right panels. **(D)** Immunostaining for tdTomato and pericyte marker PDGFRb shows that *Sox9-CreER* labels most PDGFRb$^+$ pericytes at P19. Arrowheads indicate tdTomato$^+$PDGFRb$^+$ pericytes. **(E)** Immunostaining for tdTomato and aSMA shows that *Sox9-CreER* labels most aSMA$^+$ smooth muscle cells at P19. Arrowheads indicate tdTomato$^+$aSMA$^+$ smooth muscle cells. Scale bar, 100 μm. LV, left ventricle.

EFE fibroblasts, we developed an EFE-like model using *Sox9-CreER;R26-tdTomato* donor hearts. Similar to the native heart study, tamoxifen was administered at E9.5 to label MCs in donor hearts. Donor hearts were collected and implanted in recipient mice at P7. At day 12 following transplantation, the donor hearts were harvested and analyzed (Figure 4A). Immunostaining for tdTomato and PDGFRa showed that the majority of PDGFRa$^+$ fibroblasts within the EFE-like tissues were tdTomato$^+$ (88.68% ± 0.98%; n = 5; Figure 4B-4D). We also carried out flow cytometry analysis to study the percentage of tdTomato$^+$ fibroblasts in the EFE-like model, and found that 84.85% ± 0.98% of PDGFRa$^+$ fibroblasts were labeled by tdTomato (Figure 4E-4G). To further confirm if MCs give rise to fibroblasts, we also co-stained for an additional fibroblast marker FSP1, and detected tdToma-

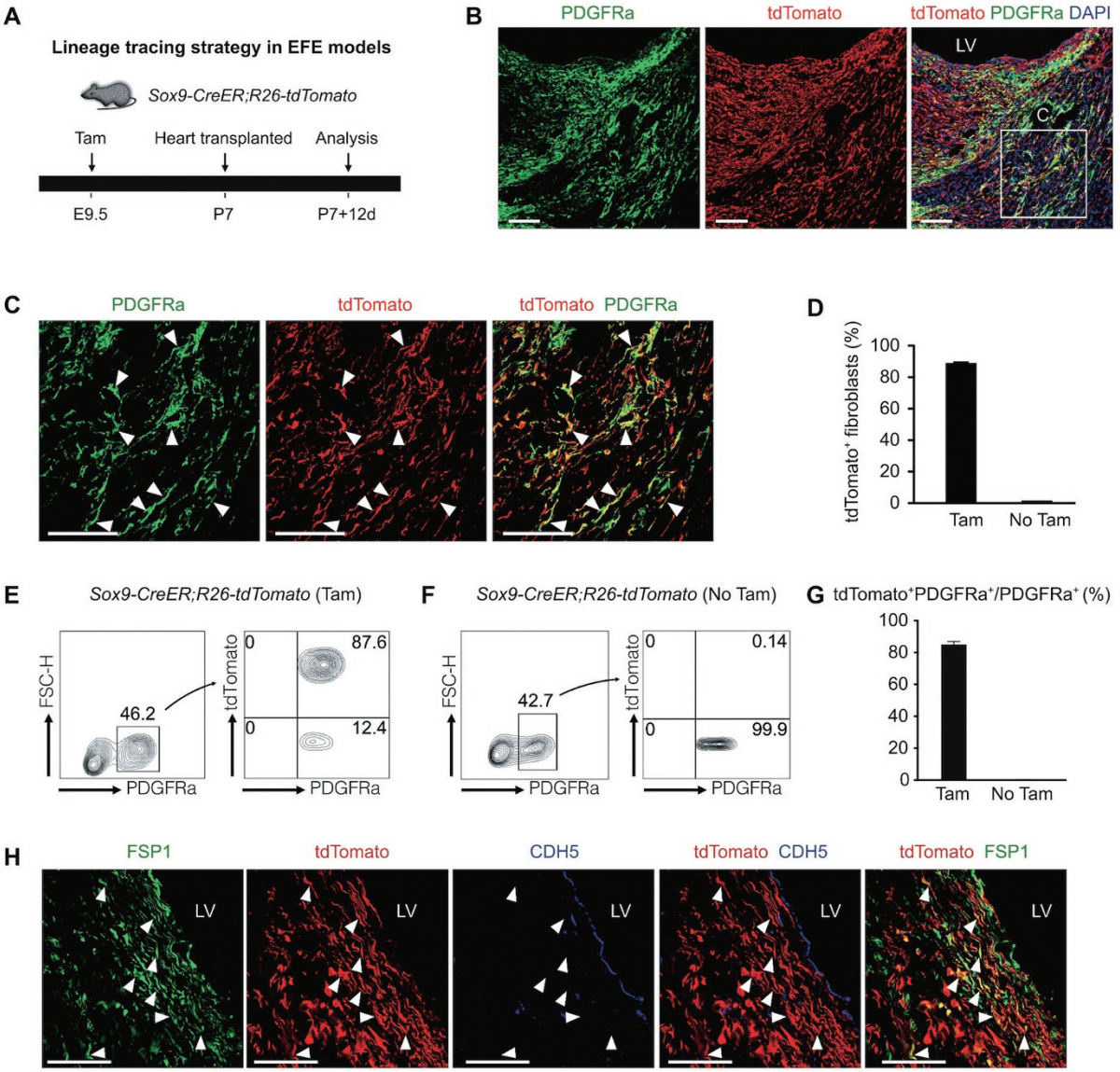

Figure 4 Embryonic cardiac mesenchymal cells (MCs) contribute to the majority of fibroblasts in the EFE-like tissues. **(A)** Schematic showing strategy for labeling embryonic cardiac MCs using *Sox9-CreER;R26-tdTomato* mice. Tamoxifen was administered at E9.5 and hearts were collected and transplanted into recipients at P7. The donor hearts were collected for analysis at day 12 following transplantation. **(B, C)** Immunostaining for tdTomato and PDGFRa shows that tdTomato labels PDGFRa$^+$ fibroblasts (arrowheads) in the EFE-like tissues. Boxed region in **B** is magnified in **C**. **(D)** Quantification of the percentage of tdTomato$^+$PDGFRa$^+$ fibroblasts within the EFE-like tissues (n = 5). **(E, F)** Representative flow cytometric analysis of the percentage of tdTomato labeled PDGFRa$^+$ cells within the EFE-like hearts. **(G)** Quantification results of tdTomato labeled PDGFRa$^+$ cells within the EFE-like models by flow cytometric analysis. For each group, n = 4. **(H)** Immunostaining for tdTomato, CDH5 and FSP1 shows that tdTomato labels FSP1$^+$CDH5$^-$ cells (arrowheads) within the EFE-like tissues. Scale bars, 100 μm. LV, left ventricle.

to$^+$FSP1$^+$CDH5$^-$ fibroblasts within the EFE-like tissues (Figure 4H). Our results suggested that most EFE fibroblasts were derived from *Sox9-CreER*-labeled embryonic MCs.

Embryonic endocardium minimally contributes to the EFE fibroblasts

As cardiac MCs include Endo-MCs and Epi-MCs, we asked to what extent these MCs from each respective compartment contribute to fibroblasts within EFE-like tissues. To address this question, we employed endocardial- and epicardial-specific inducible Cre lines for fate

mapping analysis on their descendants in EFE-like models.

Cardiac endocardium represents a unique population of endothelial cells that expresses NFATC1 at early embryonic stages [38-40]. For tracing the descendants of embryonic endocardium including Endo-MCs, we generated a tamoxifen-inducible *Nfatc1-2A-CreER* knock-in line (Supplementary information, Figure S6A). First, we analyzed expression of ESR, which is a surrogate for NFATC1 expression. Whole-mount staining showed that ESR was expressed in the endocardium of *Nfatc1-2A-CreER* embryos at E8.5 (Supplementary information, Figure S6B). Immunostaining for ESR and CDH5 revealed that ESR expression was specific to the endocardial cells at E9.5 (Supplementary information, Figure S6C). Next, to determine the Endo-MCs labeling by *Nfatc1-2A-CreER*, we performed lineage tracing experiments by crossing *Nfatc1-2A-CreER* with the reporter *R26-tdTomato* line. Tamoxifen was administered at E8.5 and embryos were collected at E10.5 (Supplementary information, Figure S6D). Co-staining for tdTomato and the endothelial cell marker PECAM on E10.5 embryonic sections showed that *Nfatc1-2A-CreER* labeled endocardial cells and endocardial-derived cushion mesenchymal cells (Supplementary information, Figure S6E). We also followed the fate of Nfatc1-derived cells to the postnatal stage, and collected *Nfatc1-2A-CreER;R26-tdTomato* hearts at P19 (Supplementary information, Figure S6D). Immunostaining for tdTomato and the fibroblast marker PDGFRa on heart sections showed that a subset of tdTomato$^+$ cells were PDGFRa$^+$ and these were distributed within atrioventricular valves, the ventricular septum and the subendocardial myocardium (Supplementary information, Figure S6F-S6H). Our results are consistent with a recent study of the endocardial origin of cardiac fibroblasts [19].

To examine the endocardial contribution to EFE fibroblasts, we developed EFE-like models using *Nfatc1-2A-CreER;R26-tdTomato* heart transplantation (Figure 5A). On the EFE heart sections, we co-stained tdTomato and PDGFRa, and identified tdTomato$^+$PDGFRa$^+$ fibroblasts in the subendocardial EFE-like tissues (Figure 5B). Quantification of the percentage of labeled fibroblasts within the EFE-like tissues showed that 5.96% ± 0.74% of fibroblasts were derived from the *Nfatc1-2A-CreER*-labeled embryonic endocardium (Figure 5C). Immunostaining for FSP1 and CDH5 also identified endocardial-derived tdTomato$^+$FSP1$^+$CDH5$^-$ cells (Figure 5D). We also carried out flow cytometric analysis to study the percentage of tdTomato$^+$ fibroblasts within the EFE-like model, and found that about 8.20% ± 0.41% of PDGFRa$^+$ fibroblasts were labeled by tdTomato (Figure 5E-5G). To test how endocardial-derived fibroblasts respond to injury, we collected donor hearts at day 3 post transplantation, and stained for tdTomato, PDGFRa and proliferation marker Ki67 (Figure 5H). Expression of Ki67 in tdTomato$^+$ fibroblasts suggested that EndMT-derived fibroblasts proliferated resulting in excessive fibrosis in EFE.

We next employed another inducible Cre line *Npr3-CreER* that specifically labels the embryonic endocardium for analysis in the EFE-like model (Figure 6A). Co-staining of tdTomato and PDGFRa on the donor heart sections of *Npr3-CreER;R26-tdTomato* showed that tdTomato labeled some PDGFRa$^+$ fibroblasts within the EFE-like tissues (Figure 6B). Quantification of the percentage of tdTomato$^+$ cells in the PDGFRa$^+$ population within the EFE-like tissues showed that 10.41% ± 2.41% of fibroblasts were derived from the *Npr3-CreER*-labeled embryonic endocardium (Figure 6C). Immunostaining for FSP1 and CDH5 on EFE heart sections of *Npr3-CreER;R26-tdTomato* also identified a small number of tdTomato$^+$FSP1$^+$CDH5$^-$ cells within the EFE-like tissues (Figure 6D). Flow cytometric analysis of the percentage of tdTomato-labeled PDGFRa$^+$ cells in the EFE-like models showed that about 8.12% ± 0.28% fibroblasts were derived from the *Npr3-CreER*-labeled embryonic endocardium (Figure 6E-6G). Immunostaining for tdTomato, PDGFRa and Ki67 on the sections of *Npr3-CreER;R26-tdTomato* donor hearts, which were collected at day 3 post transplantation, showed proliferation of embryonic EndMT-derived fibroblasts after injury (Figure 6H). Taken together, our results demonstrated that the embryonic endocardium contributed to EFE fibroblasts, and their contribution (about 6-10%) did not represent a major source of EFE fibroblasts.

Embryonic epicardium contributes to the majority of EFE fibroblasts

As embryonic endocardium minimally contributed to EFE fibroblasts, we hypothesized that the embryonic epicardium (Epi-MCs) differentiated into the majority of fibroblasts within EFE-like tissues. To test this, we crossed the epicardial Cre line *Wt1-CreER* [16] with the reporter line *R26-tdTomato* and examined the lineage conversion of epicardium in the EFE-like model. First, we performed fate mapping of the embryonic epicardium in native hearts. Tamoxifen was administered at E10.5 and the hearts were harvested and analyzed at P19 (Figure 7A). Immunostaining for tdTomato and PDGFRa was performed on heart sections of *Wt1-CreER;R26-tdTomato*. We found that the majority of PDGFRa$^+$ fibroblasts in the ventricles were tdTomato$^+$ (86.63% ± 2.87%, Figure 7B). These data suggested that the embryonic epicardium was the major source of fibroblasts in native hearts, which is

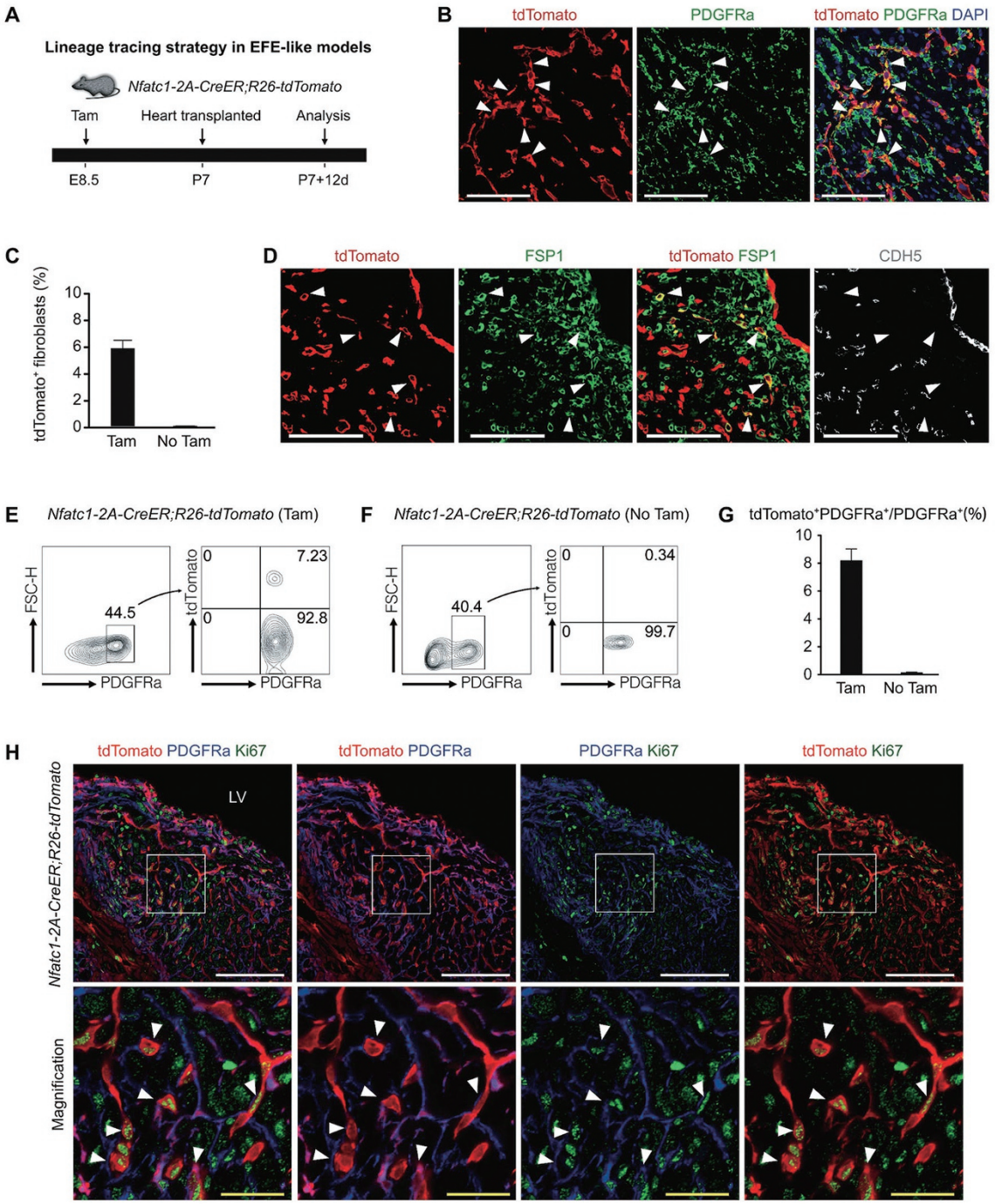

Figure 5 *Nfatc1-2A-CreER*-labeled embryonic endocardial cells contribute to fibroblasts in the EFE-like tissues. **(A)** Schematic showing strategy for lineage tracing of embryonic endocardial cells in an EFE-like model using *Nfatc1-2A-CreER;R26-tdTomato* mice. **(B)** Immunostaining for tdTomato and PDGFRa on heart sections shows that a subset of PDGFRa$^+$ fibroblasts was tdTomato$^+$ (arrowheads) in the EFE-like tissues. **(C)** Quantification of the percentage of tdTomato$^+$PDGFERa$^+$ fibroblasts within the EFE-like tissues. n = 5. **(D)** Immunostaining for tdTomato and FSP1 on heart sections shows that a subset of FSP1$^+$ cells were tdTomato$^+$ in the EFE-like tissues. Arrowheads indicate tdTomato$^+$FSP1$^+$CDH5$^-$ cells. **(E, F)** Representative flow cytometric analysis of the percentage of tdTomato$^+$ fibroblasts in the EFE-like model. **(G)** Quantification results of tdTomato-labeled PDGFRa$^+$ cells within the EFE-like model by flow cytometric analysis. For each group, n = 4. **(H)** Immunostaining for tdTomato, PDGFRa and Ki67 on sections of the EFE-like hearts from *Nfatc1-2A-CreER;R26-tdTomato* mice. The mice were treated with tamoxifen at E8.5. The donor hearts were transplanted at P7 and collected at day 3 post transplantation. The arrowheads indicate tdTomato$^+$PDGFRa$^+$Ki67$^+$ cells. Scale bars, white, 100 μm; yellow, 25 μm. LV, left ventricle.

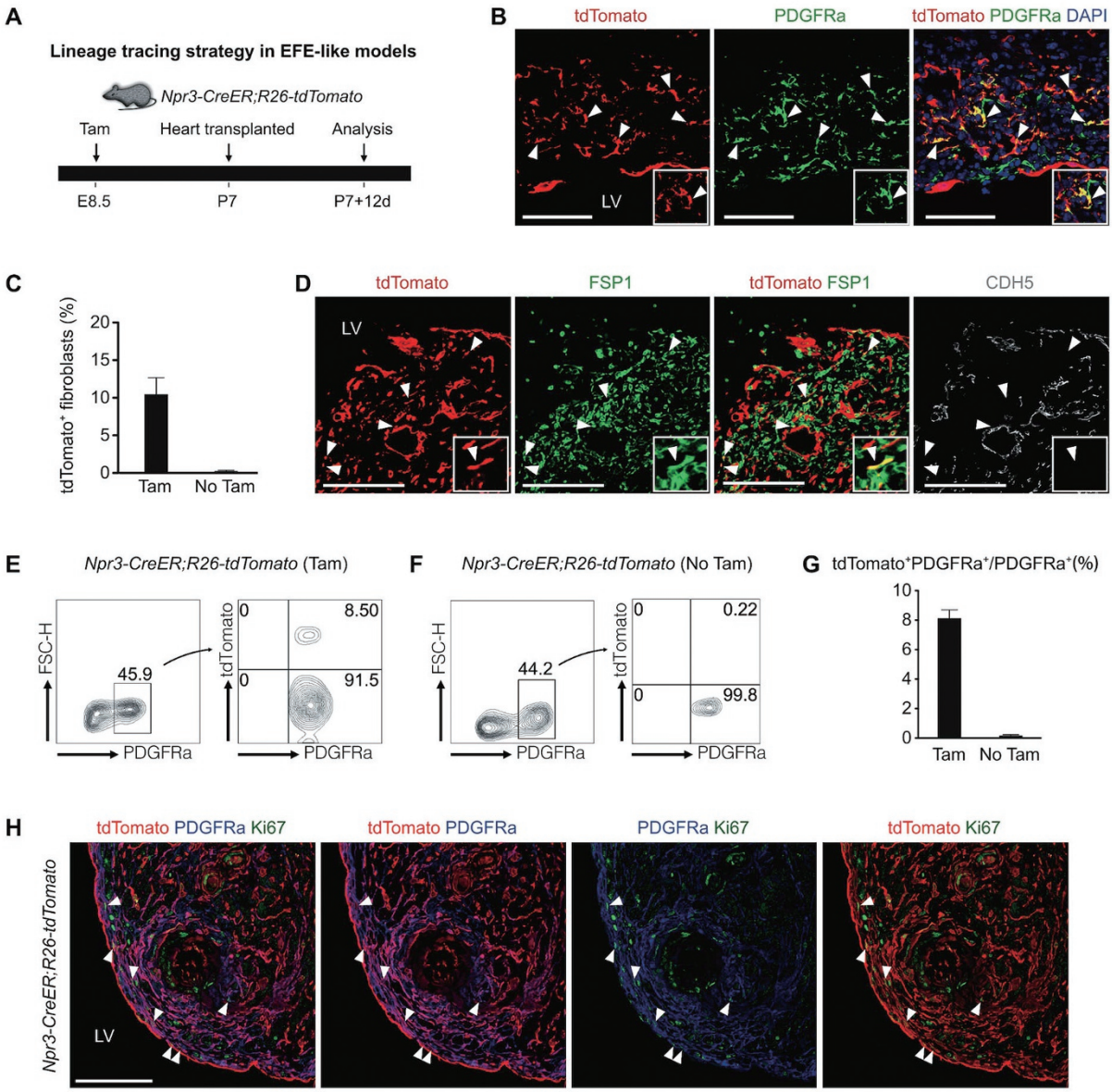

Figure 6 *Npr3-CreER*-labeled embryonic endocardial cells contribute to fibroblasts within the EFE-like tissues. **(A)** Schematic showing the strategy for lineage tracing of embryonic endocardial cells in the EFE-like model using *Npr3-CreER;R26-tdTomato* mice. **(B)** Immunostaining for tdTomato and PDGFRa on heart sections shows that a subset of PDGFRa$^+$ fibroblasts were tdTomato$^+$ (arrowheads) within the EFE-like tissues. **(C)** Quantification of the percentage of tdTomato$^+$PDGFRa$^+$ fibroblasts in the EFE-like tissues. n = 5. **(D)** Immunostaining for tdTomato and FSP1 on heart sections shows that a subset of FSP1$^+$ cells were tdTomato$^+$ within the EFE-like tissues. The arrowheads indicate tdTomato$^+$FSP1$^+$CDH5$^-$ cells. **(E, F)** Representative flow cytometric analysis of the percentage of tdTomato$^+$ fibroblasts in the EFE-like model. **(G)** Quantification results of tdTomato$^+$ fibroblasts within the EFE-like model by flow cytometric analysis. For each group, n = 4. **(H)** Immunostaining for tdTomato, PDGFRa and Ki67 on sections of the EFE-like hearts from *Npr3-CreER;R26-tdTomato* mice. The mice were treated with tamoxifen at E8.5. The donor hearts were transplanted at P7 and collected at day 3 post transplantation. The arrowheads indicate tdTomato$^+$PDGFRa$^+$Ki67$^+$ cells. Scale bars, 100 μm. LV, left ventricle.

in accordance with previous studies [15, 37, 41]. We then developed EFE-like models using *Wt1-CreER;R26-tdTomato* mice and examined the contribution of embryonic epicardium to EFE fibroblasts (Figure 7C). Co-staining of tdTomato and PDGFRa showed the co-localization of tdTomato and PDGFRa within the EFE-like tissues (Figure 7D). Immunostaining for tdTomato, FSP1 and CDH5 also identified tdTomato$^+$FSP1$^+$CDH5$^-$ cells

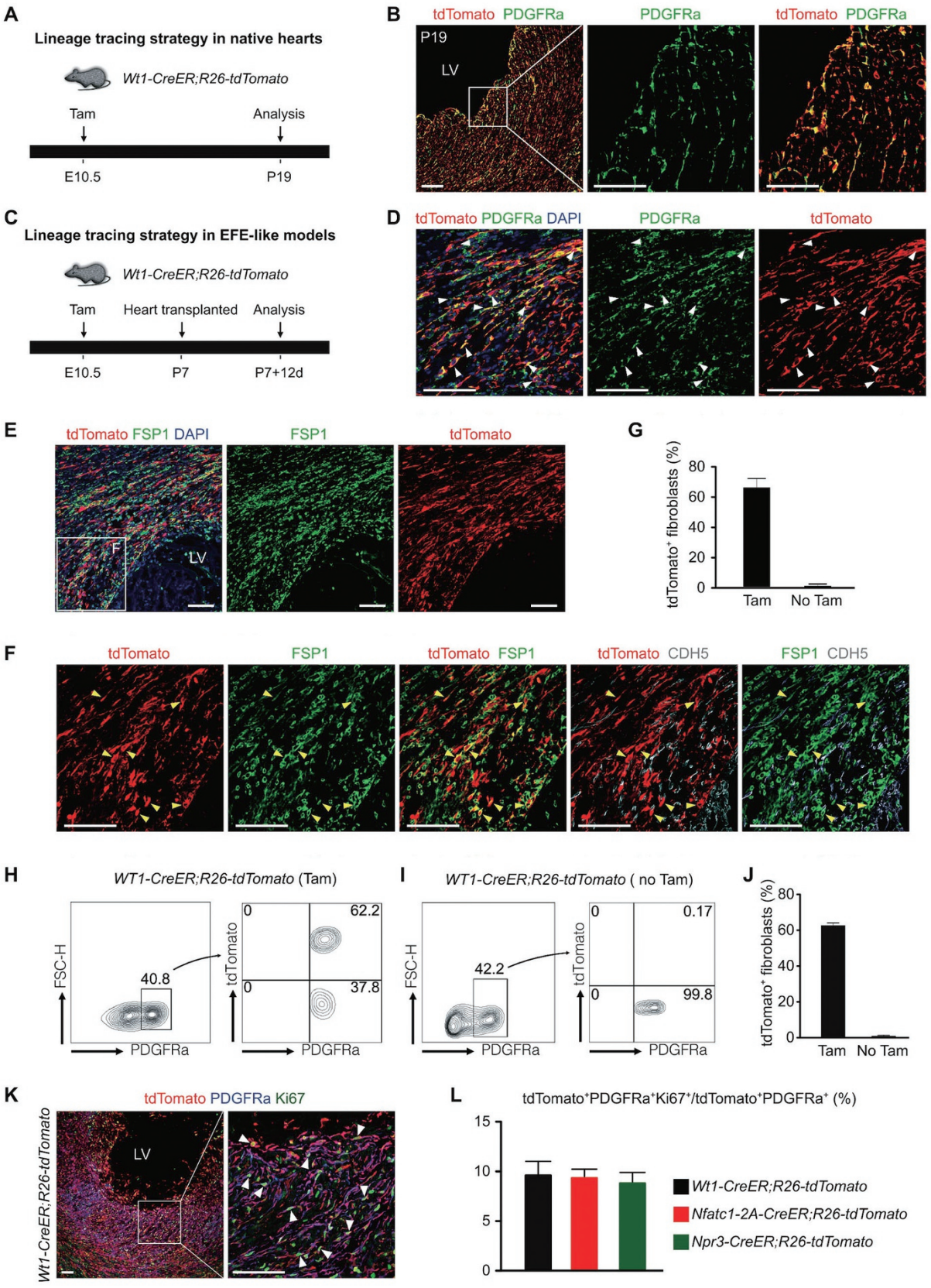
A
Lineage tracing strategy in native hearts
Wt1-CreER;R26-tdTomato
Tam
Analysis
E10.5
P19
B
tdTomato PDGFRa
PDGFRa
tdTomato PDGFRa
P19
LV
C
Lineage tracing strategy in EFE-like models
Wt1-CreER;R26-tdTomato
Tam
Heart transplanted
Analysis
E10.5
P7
P7+12d
D
tdTomato PDGFRa DAPI
PDGFRa
tdTomato
E
tdTomato FSP1 DAPI
FSP1
tdTomato
F
LV
G
tdTomato+ fibroblasts (%)
80
60
40
20
0
Tam
No Tam
F
tdTomato
FSP1
tdTomato FSP1
tdTomato CDH5
FSP1 CDH5
H
WT1-CreER;R26-tdTomato (Tam)
FSC-H
40.8
PDGFRa
tdTomato
0
62.2
0
37.8
PDGFRa
I
WT1-CreER;R26-tdTomato (no Tam)
FSC-H
42.2
PDGFRa
tdTomato
0
0.17
0
99.8
PDGFRa
J
tdTomato+ fibroblasts (%)
80
60
40
20
0
Tam
No Tam
K
tdTomato PDGFRa Ki67
Wt1-CreER;R26-tdTomato
LV
L
tdTomato+PDGFRa+Ki67+/tdTomato+PDGFRa+ (%)
15
10
5
0
Wt1-CreER;R26-tdTomato
Nfatc1-2A-CreER;R26-tdTomato
Npr3-CreER;R26-tdTomato

within the subendocardial EFE-like tissues of the left ventricles (Figure 7E and 7F). Quantification of the percentage of tdTomato$^+$PDGFRa$^+$ cells in the EFE-like tissues showed that 65.10% ± 8.55% of fibroblasts were derived from *Wt1-CreER*-labeled embryonic epicardium and their derivatives (Figure 7G). Flow cytometric analysis showed that 62.58% ± 0.71% of PDGFRa$^+$ cells were labeled by tdTomato (Figure 7H-7J). Immunostaining for tdTomato, PDGFRa and Ki67 on the sections of *Wt1-CreER;R26-tdTomato* donor hearts, which were collected at day 3 post transplantation, also confirmed proliferation of EpiMT-derived fibroblasts after injury (Figure 7K). Taken together, our results demonstrated that the majority of fibroblasts within EFE-like tissues originated from the epicardium. We also compared the proliferation rates of epicardial- and endocardial-derived fibroblasts at day 3 post transplantation, and did not find a significant difference (Figure 7L), which suggests that both EpiMT- and EndMT-derived fibroblasts responded to the injury and contributed to the fibrosis formation. Indeed, our results are consistent with previous work [21].

Postnatal epicardium does not give rise to EFE fibroblasts

Previous lineage tracing data suggested that *Npr3-CreER*-labeled postnatal endocardium and epicardium did not contribute to EFE fibroblasts (Figure 1D-1F; Supplementary information, Figure S2A and S2B). To further examine whether postnatal epicardium generates EFE fibroblasts, we traced the fate of postnatal epicardium using *Wt1-CreER;R26-tdTomato* mice. To test the labeling of *Wt1-CreER;R26-tdTomato* in native postnatal hearts, tamoxifen was administered at P5 and hearts were harvested at P19 (Figure 8A). Immunostaining for tdTomato and PECAM on heart sections showed that *Wt1-CreER* labeled epicardial cells and some coronary endothelial cells (Figure 8B). Immunostaining for PDGFRa and tdTomato on heart sections showed that *WT1-CreER* did not label fibroblasts at the postnatal stages (Figure 8C). Next, we developed the EFE-like model using *Wt1-CreER;R26-tdTomato* mice. Tamoxifen was administered at P5, and hearts were collected and implanted at P7. At day 12 following transplantation, the donor *Wt1-CreER;R26-tdTomato* hearts were harvested and analyzed (Figure 8D). Immunostaining for tdTomato, CDH5 and PDGFRa on the EFE heart sections showed that tdTomato$^+$ cells within the EFE-like tissues were CDH5$^+$ but PDGFRa$^-$ (Figure 8E and 8F). Our results suggested that the postnatal epicardium did not contribute to EFE fibroblasts.

Blocking the TGFβ signaling pathway effectively reduces fibroblast accumulation in EFE-like model

The TGFβ pathway has been reported to be a key mediator for cardiac fibroblast activation and shown to play important roles in cardiac fibrosis [42, 43]. Previous gain- and loss-of-function studies have demonstrated the pivotal role of TGFβ in inducing fibrosis [44-47]. Similarly, inhibition of TGFβ has been shown to ameliorate fibrosis [43, 48]. To test whether TGFβ signaling participates in fibroblast accumulation or fibrosis formation in the EFE-like model, we stained with anti-TGFβ1 and anti-TGFβ2 antibodies on the sections of native hearts and EFE-like hearts. In the native hearts at P19, neither TGFβ1 nor TGFβ2 was detected in the myocardium (Figure 9A). However, expression of TGFβ1 and TGFβ2 was significantly higher in the myocardium of left ventricles from the EFE-like hearts (Figure 9A). As an internal control, we have also checked the level of TGFβ in the right ventricle. Our results showed that the expression level of TGFβ1 and TGFβ2 was much lower in the right ventricles compared to that of the left ventricles (Figure 9A and 9B), which could partially explain why excessive fibrosis often occurs in the left ventricles rather than the right ventricles in EFE patients and EFE-like models.

Previous studies reported that bone morphogenetic protein 7 (BMP7) could antagonize the TGFβ signaling pathway through a direct Smad-dependent counteraction [13, 22, 49]. We therefore treated the recipient mice

Figure 7 Embryonic epicardial cells contribute to the fibroblasts within the EFE-like tissues. **(A)** Schematic showing strategy for lineage tracing of embryonic epicardial cells in native hearts using *Wt1-CreER;R26-tdTomato* mice. **(B)** Immunostaining for tdTomato and PDGFRa on heart section shows that the majority of PDGFRa$^+$ fibroblasts are tdTomato$^+$. **(C)** Schematic showing the strategy for lineage tracing of embryonic epicardial cells in the EFE-like model using *Wt1-CreER;R26-tdTomato* mice. **(D)** Immunostaining for tdTomato and PDGFRa on heart sections showed PDGFRa$^+$ fibroblasts were tdTomato$^+$ (arrowheads) in the EFE-like tissues. **(E**, **F)** Immunostaining for tdTomato and FSP1 on heart sections. Boxed region in **E** is magnified in **F**. Yellow arrowheads indicate tdTomato$^+$FSP1$^+$CDH5$^-$ cells. **(G)** Quantification of the percentage of tdTomato$^+$PDGFRa$^+$ fibroblasts. **(H**, **I)** Representative flow cytometric analysis of the percentage of tdTomato$^+$PDGFRa$^+$ fibroblasts in the EFE-like model. **(J)** Quantification results of tdTomato$^+$PDGFRa$^+$/PDGFRa$^+$ within the EFE-like model by flow cytometric analysis. *n* = 5. **(K)** Immunostaining for tdTomato, PDGFRa and Ki67 on sections of the EFE-like hearts from *Wt1-CreER;R26-tdTomato* mice. The mice were administered with tamoxifen at E10.5. The donor hearts were transplanted at P7 and collected at day 3 post transplantation. The arrowheads indicate tdTomato$^+$PDGFRa$^+$Ki67$^+$ cells. **(L)** Quantification of the percentage of proliferating fibroblasts from different origins. Scale bars, 100 μm. LV, left ventricle; RV, right ventricle.

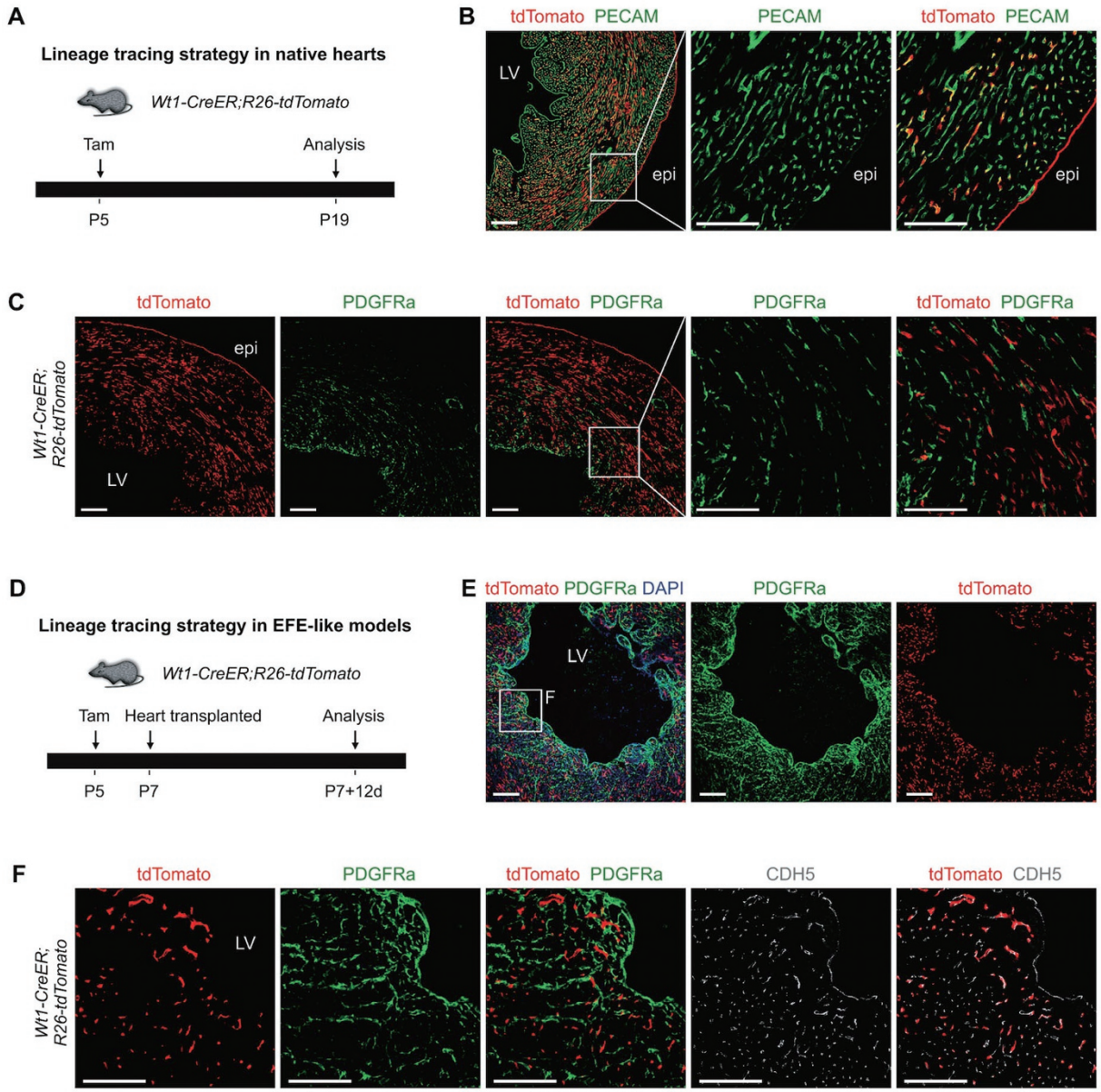

Figure 8 Postnatal epicardial cells do not contribute to the fibroblasts within the EFE-like tissues. **(A)** Schematic figure showing the strategy for lineage tracing of epicardial cells in native hearts at postnatal stage using *Wt1-CreER*;*R26-tdTomato* mice. **(B)** Immunostaining for tdTomato and PECAM on heart sections shows that postnatal *Wt1-CreER* labels coronary endothelial cells and epicardial cells. **(C)** Immunostaining for tdTomato and PDGFRa shows that *Wt1-CreER* does not label PDGFRa$^+$ fibroblasts at postnatal stage. **(D)** Schematic figure showing the lineage tracing strategy of postnatal epicardial cells in the EFE-like model using *Wt1-CreER*;*R26-tdTomato* mice. **(E,F)** Immunostaining for tdTomato and PDGFRa on heart sections shows that *Wt1-CreER* labeled cells (including epicardial cells and some endothelial cells) do not contribute to PDGFRa$^+$ fibroblasts within the EFE-like tissues. Boxed region in **E** is shown in **F**. Scale bar, 100 μm. epi, epicardium; LV, left ventricle.

with BMP7 (30 μg/kg) on every alternate day following transplantation. At day 12 post transplantation, we collected the EFE-like hearts and performed sirius red staining, and found that the accumulation of fibroblasts within EFE-like hearts was significantly reduced after BMP7 administration compared to that of the control group (Figure 9C and 9D). PDGFRa staining also confirmed less fibroblast accumulation in the left ventricles after BMP7 treatment (Figure 9E). Taken together, our results show that TGFβ plays a pivotal role in fibroblast accumulation and inhibition of the TGFβ signaling could ameliorate fibrosis in the EFE-like model.

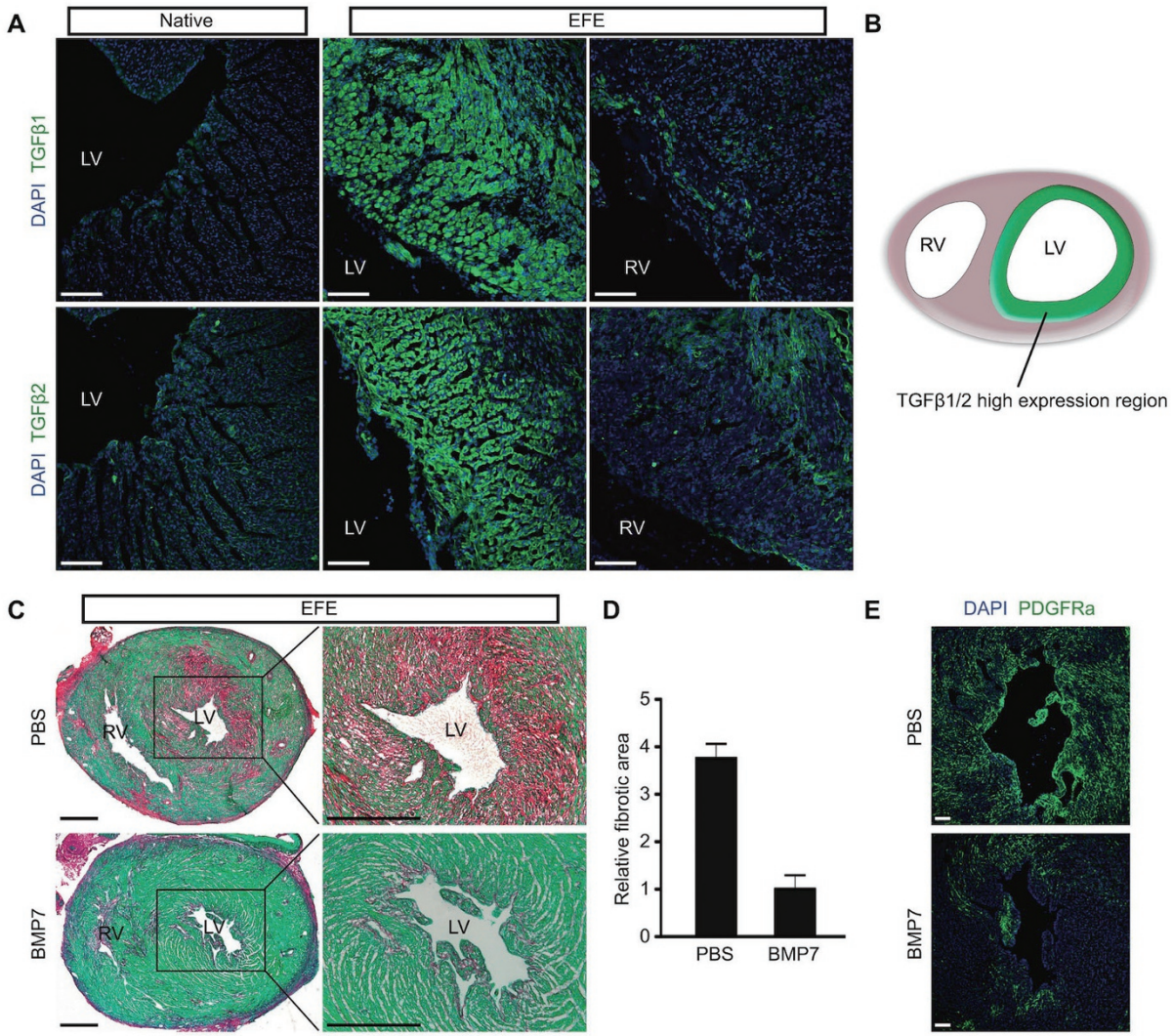

Figure 9 Blocking TGFβ signaling pathway reduces fibroblast accumulation within the EFE-like model. **(A)** Immunostaining for TGFβ1 or TGFβ2 shows that both TGFβ1 and TGFβ2 are highly expressed in the left ventricles of EFE-like models. Scale bar, 100 μm. **(B)** Cartoon shows that TGFβ1 and TGFβ2 are highly expressed in the EFE-like tissue. **(C)** Representative sirius red staining on sections of the EFE-like hearts, which were treated with PBS or BMP7. Scale bars, 500 μm. **(D)** Quantification results of the relative fibrotic area of the EFE-like hearts, which are treated with PBS or BMP7. $P < 0.05$. For each group, $n = 7$. **(E)** Immunostaining for PDGFRa on sections of the EFE-like hearts, which were treated with PBS or BMP7. Scale bars, 100 μm. LV, left ventricle. RV, right ventricle.

Discussion

EFE refers to a specialized type of fibrosis with excessive fibroblasts deposited in the thickened subendocardial layer. During EFE, proliferation of fibrous and elastic tissues may eventually lead to decreased compliance and impaired diastolic functions [6]. These excessive fibroblasts are mainly restricted to the subendocardial layer rather than throughout the myocardium. As indicated by its name endocardial fibroelastosis, EFE, is thought to be largely associated with endocardial cells and/or their derivatives, such as excessive fibroblast formation from endocardial to mesenchymal transition [13]. Here, we provide direct genetic lineage tracing evidence that, rather than the endocardium, the epicardium and its derived mesenchymal cells (Epi-MCs) contributed to the majority of fibroblasts within EFE-like tissues. These Epi-MCs populated the myocardium at the embryonic stage and generated excessive fibroblasts within EFE-like tissues at the postnatal stage. Unexpectedly, the endocardium contributed minimally to fibroblasts within EFE-like tissues. Rather than postnatal endocardial to mesenchymal

transition, endocardial cells generated Endo-MCs at the embryonic stage and it was such MCs that contributed to fibroblast formation in postnatal EFE. Our study has discovered a new, major cellular origin of EFE and it suggests that the location of pathogenesis might not reflect its cellular origin. We also found that TGFβ1 and TGFβ2 were highly expressed in the myocardium of left ventricle and that inhibition of the TGFβ signaling with BMP7 ameliorated fibrosis in the EFE-like model. Our comprehensive lineage tracing studies from developmental to pathogenetic stages provide new insights into understanding the fundamental pathomechanisms underlying EFE.

In this study, we used an established EFE-like model [13, 28]. This transplant model may create a cardiac pathology resembling human EFE, but it is still unknown if the underlying pathobiology of this model can accurately recapitulate human EFE. There are some differences between this model and human EFE, such as lack of cardio-respiratory coupling and negative intrathoracic pressures affecting the heart. Therefore, we term this transplant model as an "EFE-like" model. Further investigations are needed to extrapolate our findings to the clinical settings of human EFE. Even though this model has been developed and studied for years, there remains a paucity of investigation into the mechanism underlying fibrosis in the EFE-like model. Fibrosis can be a result of tissue ischemia with reduced blood flow into the hemodynamically unloaded heart. Moreover, inflammatory responses within the heart could also lead to proliferation and migration of mesenchymal cells that deposit extracellular matrix [8, 50, 51]. Nevertheless, we could not exclude the possible effects of the immune responses in the EFE-like model. Other causes such as nutrient deprivation may also be responsible for the fibrosis. Thus the precise cellular and molecular mechanisms underlying fibrosis in EFE merit further investigation with an improved model system.

As different origins of cells may determine distinct potential therapeutic targets, it is important to revisit the cellular origin of fibroblasts within the EFE-like tissues. Lineage tracing technology has been utilized to uncover the cellular origin and cell fate determination during development and diseases [52]. We took advantage of the bacteriophage Cre-Loxp system to permanently label Cre-expressing cells and all of their descendants [53]. By virtue of the constitutively active Cre lines (such as *Tie2-Cre*), any cells that expressed Cre from early development would be irreversibly labeled, thus constitutively active Cre lines do not allow us to distinguish the postnatal cell fate transition from early developmental lineage conversion [54]. A recent study using the constitutive *Tie2-Cre* reported that fibroblasts within EFE-like tissues originate from endothelial cells via aberrant EndMT [13]. It should be noted that *Tie2-Cre* labels not only postnatal endocardial cells, but also embryonic endocardial cells during early development and their derivatives such as Endo-MCs [55]. Indeed, *Tie2-Cre* labeled endocardial cells that undergo EndMT and convert into primitive mesenchymal progenitors expressing PDGFRa and PDGFRb [20]. These endocardial-derived MCs contribute to pericytes, vascular SMCs and a few fibroblasts in the developing heart at later embryonic stages [19, 20]. Thus a previous study employing *Tie2-Cre* [13] could not distinguish postnatal endocardial cells from early endocardium-derived MCs. In addition, *Tie2-Cre* labels both coronary vascular endothelial cells and endocardial cells, and it is hard to distinguish whether fibroblasts are derived from pre-existing endocardial cells or vascular endothelial cells [13]. Indeed, recent work reported that endocardium-derived fibroblasts labeled by *Tie2-Cre* and epicardium-derived fibroblasts proliferate and respond similarly to cardiac injury [21]. From temporal and spatial perspectives, it is critical to employ mouse lines that harbor inducible Cre recombinase under endocardium-specific promoter to address if postnatal endocardial cells give rise to excessive fibroblasts within EFE-like tissues.

To readdress the cellular origin of EFE fibroblasts, we generated new mouse lines for inducible lineage tracing with temporal and spatial control of Cre activity. By using the inducible endocardial Cre line *Npr3-CreER* [31, 32], we genetically labeled endocardial cells at P5 and found that most endocardial cells did not contribute to fibroblasts within EFE-like tissues. We further confirmed this finding by using the endothelial cell tracing line *Cdh5-CreER*, which labeled both endocardial cells and vascular endothelial cells with high efficiency. These data convincingly demonstrated that postnatal endocardial cells did not generate fibroblasts within EFE-like tissues. Furthermore, we identified Sox9-derived MCs at the embryonic stage and our fate mapping data showed that most fibroblasts within EFE-like tissues were derived from Sox9-derived MCs. By using *Nfatc1-2A-CreER*, *Npr3-CreER* or *Wt1-CreER* lines that respectively labeled endocardial or epicardial cells, respectively, we found that the majority of EFE fibroblasts were derived from the embryonic epicardium rather than embryonic endocardium. Collectively, these inducible lineage tracing lines with more restricted spatial and temporal Cre activity presented a new model that the resident epicardium-derived MCs, but not the endocardial cells, were the major source of EFE fibroblasts (Figure 10).

Another issue that needs to be addressed for lineage

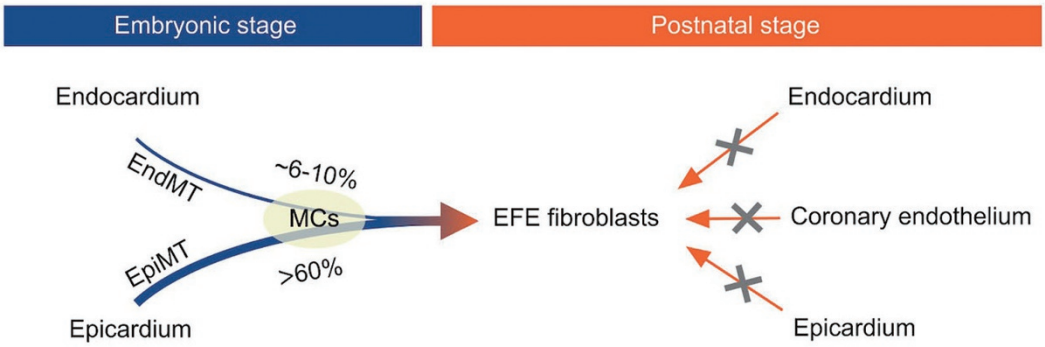

Figure 10 Proposed model for EFE fibroblast origins based on genetic lineage tracing in this study. Majority of subendocardial EFE fibroblasts are derived from embryonic MCs, which are derivatives of endocardium via EndMT and epicardium via EpiMT. Inducible lineage tracing studies showed that the embryonic epicardium is the major source for EFE fibroblasts (> 60%), while the embryonic endocardium contribute to minority of EFE fibroblasts (~6%-10%). Neither postnatal epicardial cells nor endothelial cells (including endocardium and coronary endothelium) contribute to EFE fibroblasts.

tracing is the specificity of fibroblast markers. Recent studies suggested that several molecular markers used to define fibroblasts are either non-specific or only specific for certain subsets of fibroblast population rather than the whole-fibroblast pool. Such issues could account for results of the discordant origin mentioned in above studies [56]. For instance, the typical fibroblast marker vimentin has also been found to be expressed by other cell types, including endothelial cells [57, 58]. Another marker discoidin domain receptor 2 is also expressed by both SMCs and leukocytes [59, 60]. Collagens such as Collagen1A1 are more enriched in fibrosis tissues. However, collagens are extracellular matrix proteins and are not suitable for localizing fibroblasts with lineage reporter proteins. Collagen1A1-GFP fusion reporter driven by endogenous gene could be helpful to specifically label fibroblasts [19]. Furthermore, periostin, which is also supposed to label activated fibroblasts, is, in fact, an extracellular matrix protein [61]. aSMA is supposed to be highly expressed by activated fibroblasts termed "myofibroblasts". However, aSMA is also highly expressed by SMCs, and labels only 15% of collagen-positive cells as fibrosis tissues [19, 62]. FSP1 and thymus cell antigen-1 are putative markers for subgroups of fibroblasts. However, they are also expressed by a subset of endothelial cells and leukocytes [19, 30]. Since previous work demonstrating endocardial contribution to fibroblasts mainly used FSP1 as the fibroblast cell marker [13, 22], we included FSP1 together with the endothelial cell marker CDH5 to distinguish $FSP1^+CDH5^-$ and $FSP1^+CDH5^+$ cells within EFE-like tissues. We also found that FSP1 was expressed in leucocytes and co-localized with CD45, CD11b and F4/80 in native hearts and EFE-like hearts (Supplementary information, Figure S7). Previous evidence for EndMT-derived fibroblasts was based on results of lineage tracing via *Tie2-Cre*, which actually labels both endothelial cells and resident $FSP1^+$ leucocytes [13]. Recent studies suggested that PDGFRa comprehensively and strongly marked fibroblasts [19], despite that PDGFRa is also expressed in mesenchymal stem cell-like progenitor cells of the neonatal mouse heart [63]. Therefore, we used PDGFRa as a fibroblast marker to determine the lineage of fibroblasts within fibrous EFE-like tissues.

Although we provided new evidence suggesting that embryonic epicardium and their derived MCs were the major source of EFE fibroblasts, and the TGFβ signaling pathway plays important roles in EFE formation, additional studies are needed to delineate more signals regulating expansion of epicardium-derived fibroblasts and the relationship between EFE and pathogenesis of HLHS. The signaling pathways governing Epi-MCs expansion in EFE fibrosis may include both developmental program of EpiMT as well as signals regulatory fibroblast proliferation such as Shh, Notch, PDGF and FGF [27, 37, 64-68]. Therefore, detailed molecular mechanisms regulating Epi-MCs cell fate and function merit further investigations. Together, understanding the cellular origin of EFE fibroblasts and mechanisms underlying cell fate determination and expansion could potentially uncover new therapeutic candidates for treatment of EFE.

Materials and Methods

Mice

All animal experiments were carried out in strict accordance with the guidelines in the Institutional Animal Care and Use Committee (IACUC) of the Institute for Nutritional Sciences, Shanghai Institutes for Biological Sciences, Chinese Academy of Science. Tamoxifen was administered by oral gavage at the indicated time

points (0.1-0.2 mg/g of body weight). Caesarean section was performed on pregnant mice receiving tamoxifen to obtain perinatal pups. *R26-tdTomato*, *Npr3-CreER*, *Cdh5-CreER*, *Wt1-CreER* and *Sox9-CreER* mice were described previously [16, 32, 69-71]. The *Nfatc1-2A-CreER* mouse line was generated by homologous recombination using CRISPR/Cas9 technology. The 2A peptide sequence derived from porcine teschovirus-1 was upstream of the cDNA encoding CreER and polyadenylation sequence. This 2A-CreER cassette was introduced into the 9th exon of Nfatc1, and corrected targeting was verified by long PCR genotyping. This mouse line was generated by Shanghai Biomodel Organism. Co, Ltd. All mice were maintained on the C57BL6/ICR background. Genomic DNA for genotyping was prepared from embryonic yolk sac or mouse tail. Tissues were lysed by incubation with Proteinase K overnight at 55 °C. DNA was precipitated by adding isopropanol, and washed in 70% ethanol. Then genomic DNA was diluted in 200 µl distilled water.

Animal model of unloaded heterotopic heart transplantation

The donor pups at postnatal day 7 were anesthetized by intraperitoneal injection of pentobarbital sodium, and then received 60 IU heparin. The hearts were collected through a midline thoracic incision. The vena cava, aorta and pulmonary artery were identified, isolated, ligated and transected. The donor hearts were then placed in cold high potassium Krebs-Henseleit solution as previously described until the time of implantation [72]. Seven-day-old donor hearts were implanted into the peritoneal cavity of 8-week-old ICR mice in an unloaded configuration as previously described [28, 29]. Briefly, the ascending aorta was anastomosed to the infrarenal aorta, and the pulmonary artery was anastomosed to the infrarenal vena cava. At day 12 following implantation, the recipients were sacrificed and the donor hearts were collected and analyzed. To test the fibrosis inhibition of BMP7, the recipient mice were treated with BMP7 (Abcam, ab87055) or PBS by intraperitoneal injection every other day at a concentration of 30 µg/kg since transplantation. Then the donor hearts were collected at day 12 post transplantation for analysis.

Immunofluorescent staining

Immunofluorescent staining was performed as previously described [31]. Briefly, embryonic hearts were collected and washed with PBS to remove excessive blood. After fixed in 4% PFA at 4 °C for 20 min to 1 h, tissues were dehydrated in 30% sucrose for several hours or overnight until they sank to the bottom. The tissues were embedded in OCT (Sakura) and serial cryosections of 8-10 µm thickness were collected. After air drying for 30 min, slides were blocked with PBS supplemented with 0.1% triton X-100 and 5% normal donkey serum (Jackson Immuno Research) for 30 min at room temperature, followed by incubation with the first antibody at 4 °C overnight. The following first antibodies were used: tdTomato (Rockland, 600-401-379), tdTomato (ChromoTek, ABIN334653), PECAM (BD, 553370), CDH5 (R&D, AF1002), FABP4 (Abcam, ab13979), PDGFRa (eBioscience, 14-1401-81), PDGFRa (R&D, AF1062), PDGFRb (eBioscience, 14-1402), aSMA (Sigma, F3777), ESR (Abcam, ab27595), Tbx18 (Santa Cruz, sc-17869), FSP1 (Dako, A5114), Sox9 (Millipore, AB5535), CD11b (BD, 550282), CD45 (eBioscience, 47-0451), F4/80 (Abcam, ab6640), Collagen I (Abcam, ab34710), Collagen III (Southernbiotech, 1330-01), Ki67 (Thermo Scientific, RM-9106-S0), TGFβ1 (Santa Cruz, sc-146), TGFβ2 (Abcam, ab36495), Tnni3 (Abcam, ab56357). Signals were developed with Alexa fluorescence antibodies (Invitrogen). For weak signals, we used HRP-conjugated secondary antibodies and developed using tyramide signal amplification kit (PerkinElmer). Images were acquired by Olympus confocal microscope (FV1200) or Zeiss microscope (AXIO Zoom. V16).

Whole-mount immunostaining for estrogen receptor

We performed whole-mount immunostaining as described previously [32]. Embryos were collected in PBS and fixed in 4% PFA at 4 °C overnight. The embryos were then dehydrated through a methanol gradient (25%, 50%, 75% and 100% methanol in PBS) for 15 min in each condition at room temperature. After that, the embryos were rehydrated through 100%, 75%, 50% and 25% methanol in PBS for 15 min in each condition at room temperature. After pretreatment in blocking buffer (5% donkey serum and 0.1% Triton X-100 in PBS) for 1 h at 4 °C, the embryos were incubated with ESR antibody (Abcam, ab27595) at 4 °C overnight. The embryos were then washed in 0.1% Triton X-100/PBS for four times, which each lasted for 1 h. After incubation with the secondary antibody (Vector lab, MP-7401) for 2 h at room temperature, the embryos were washed in 0.1% Triton X-100/PBS for 4 h. The ImmPACT DAB kit (Vector, sk-4150) was used to develop the color to the desired condition. Images were acquired by a Leica stereomicroscope (M165FC).

Sirius red staining and H&E staining

Hearts were collected in PBS buffer and fixed in 4% PFA at 4 °C for 1 h. The hearts were then dehydrated in 30% sucrose overnight and embedded in OCT. Serial cryosections of 8-10 µm thickness were collected. For sirius red staining, sections were re-fixed with Bouin's solution at room temperature for 12 h. Next, sections were stained with 0.1% fast green for 3 min. After pretreatment with 1% acetic acid for 1 min, the sections were stained with 0.1% sirius red solution for 1 min followed by a serial of dehydration procedures in ethanol and xylene. The slides were then mounted in Permount Mounting Medium. For H&E staining, slides were incubated in Hematoxylin A solution for 3 min, and then rinsed in running tap water for 1 min. The slides were then treated with 1% concentrated hydrochloric acid in 70% ethanol for 1 min and rinsed in running tap water for 1 min. After soaking in 1% ammonia water for 1 min and washed by running tap water, the slides were stained with Eosin-Y solution for 10 s followed by dehydration in ethanol and xylene. The slides were lastly mounted in neural balsam. Images were acquired by Zeiss microscope (AXIO Zoom. V16).

Cell isolation and fluorescence-activated cell sorting

Cells were isolated from EFE-like hearts as described previously [73]. Briefly, EFE-like hearts were dissected and carefully cut into small pieces with fine scissors. And then the hearts were digested by trypsinase and collagenase type II at 37 °C. After digestion, the lysis buffer containing cells were passed through 70-mm cell strainers. After centrifuging at 500× *g* for 3 min at 4 °C, non-cardiomyocytes were obtained in the suspension liquid. For identification of live cells, the LIVE/DEAD Fixable Violet Dead Cell Stain Kit (Life Technology, L34955, 1:1 000) was used according to the manufacturer's instruction. Then the isolated cells

were stained with PDGFRa-APC (eBioscience, 17-1401, 1:200) for 30 min. Flow cytometry was performed using a BD FACS Aria flow cytometry system (BD Biosciences, San Jose, CA, USA). Data were analyzed using FlowJo software (Tree Star, Ashland, Oregon, USA).

Statistical analysis

All data were collected from at least three independent experiments as indicated. Besides flow cytometry, we also counted the number of EFE fibroblasts via immunostaining on tissue sections. For analyzing the labeling percentage of EFE fibroblasts by tdTomato, we collected five heart samples for each experiment. At least eight tissue sections from each heart were collected for immunostaining; and images were taken with at least five fields in each section for analysis. The percentage of contribution to EFE fibroblasts was calculated as $tdTomato^{+}PDGFRa^{+}$ cells in $PDGFRa^{+}$ cells within EFE-like tissues. All data were presented as mean values ± SEM. Statistical comparisons between data sets were done by a two-sided unpaired Student's *t* test for comparing differences between two groups. $P < 0.05$ was considered to be statistically significant.

Acknowledgments

We thank Baojin Wu, Guoyuan Chen, Zhonghui Weng and Aimin Huang for the animal husbandry; and Wei Bian for his technical help. We thank Shanghai Biomodel Organism Science & Technology Development Co., Ltd for mouse generation. We thank Ralf Adams at Max Plank Institute for providing the *Cdh5-CreER* mouse line and Hongkui Zeng for reporter lines. We also thank other members of our laboratory for insightful discussion and technical help throughout this study. This work was supported by Strategic Priority Research Program of the Chinese Academy of Sciences (CAS, XDB19000000), The National key Research & Development Program of China (2017YFC1001300 and 2016YFC1300600), National Natural Science Foundation of China (91639302, 31625019, 31571503, 31501172, 31601168), Youth Innovation Promotion Association of CAS (2015218), Key Project of Frontier Sciences of CAS (QYZDB-SSW-SMC003), International Cooperation Fund of CAS, National Program for Support of Top-notch Young Professionals, Shanghai Science and Technology Commission (14JC1407300, 17ZR1449600, 17ZR1449800), Shanghai Yangfan Project (15YF1414000, 16YF1413400) and Rising-Star Program (15QA1404300), China Postdoctoral Science Foundation (2015M581669, 2016T90387, 2016LH0042), President Fund of Shanghai Institutes for Biological Sciences (SIBS), Astrazeneca, Boehringer Ingelheim, Sanofi-SIBS Fellowship and Research Grants Council of Hong Kong (24110515, 14111916).

Author Contributions

HZ and BZ conceived and designed the study, analyzed the data and wrote the manuscript. HZ, XH, KL, JT, LH, WP, QL, YL, XT, YW and Libo Z bred the mice and performed experiments. YY, HW, RH, FW, TC, QW, ZQ, Li Z and KL provided valuable comments, analyzed the data and edited the manuscript. BZ supervised the study.

Competing Financial Interests

The authors declare no competing financial interests.

References

1 Rosahn PD. Endocardial fibroelastosis: old and new concepts. *Bull NY Acad Med* 1955; **31**:453-472.
2 De Letter EA, Piette MH. Endocardial fibroelastosis as a cause of sudden unexpected death. *Am J Forensic Med Pathol* 1999; **20**:357-363.
3 Stehbens WE, Delahunt B, Zuccollo JM. The histopathology of endocardial sclerosis. *Cardiovasc Pathol* 2000; **9**:161-173.
4 Weinberg T, Himelfarb AJ. Endocardial fibroelastosis (so-called fetal endocarditis). A report of two cases occurring in siblings. *Bull Johns Hopkins Hosp* 1943; **72**:299.
5 Grellner W, Kaferstein H, Sticht G. Combination of fatal digoxin poisoning with endocardial fibroelastosis. *Forensic Sci Int* 1997; **89**:211-216.
6 Moller JH, Lucas RV Jr, Adams P Jr, Anderson RC, Jorgens J, Edwards JE. Endocardial fibroelastosis: a clinical and anatomic study of 47 patients with emphasis on its relationship to mitral insufficiency. *Circulation* 1964; **30**:759-782.
7 Gilbert-Barness E, Barness LA. Nonmalformative cardiovascular pathology in infants and children. *Pediatr Dev Pathol* 1999; **2**:499-530.
8 Lurie PR. Changing concepts of endocardial fibroelastosis. *Cardiol Young* 2010; **20**:115-123.
9 McElhinney DB, Vogel M, Benson CB, *et al.* Assessment of left ventricular endocardial fibroelastosis in fetuses with aortic stenosis and evolving hypoplastic left heart syndrome. *Am J Cardiol* 2010; **106**:1792-1797.
10 McElhinney DB, Marshall AC, Wilkins-Haug LE, *et al.* Predictors of technical success and postnatal biventricular outcome after *in utero* aortic valvuloplasty for aortic stenosis with evolving hypoplastic left heart syndrome. *Circulation* 2009; **120**:1482-1490.
11 Emani SM, Bacha EA, McElhinney DB, *et al.* Primary left ventricular rehabilitation is effective in maintaining two-ventricle physiology in the borderline left heart. *J Thorac Cardiovasc Surg* 2009; **138**:1276-1282.
12 Emani SM, McElhinney DB, Tworetzky W, *et al.* Staged left ventricular recruitment after single-ventricle palliation in patients with borderline left heart hypoplasia. *J Am Coll Cardiol* 2012; **60**:1966-1974.
13 Xu X, Friehs I, Zhong Hu T, *et al.* Endocardial fibroelastosis is caused by aberrant endothelial to mesenchymal transition. *Circ Res* 2015; **116**:857-866.
14 Merki E, Zamora M, Raya A, *et al.* Epicardial retinoid X receptor alpha is required for myocardial growth and coronary artery formation. *Proc Natl Acad Sci USA* 2005; **102**:18455-18460.
15 Cai CL, Martin JC, Sun Y, *et al.* A myocardial lineage derives from Tbx18 epicardial cells. *Nature* 2008; **454**:104-108.
16 Zhou B, Ma Q, Rajagopal S, *et al.* Epicardial progenitors contribute to the cardiomyocyte lineage in the developing heart. *Nature* 2008; **454**:109-113.
17 Wilm B, Ipenberg A, Hastie ND, Burch JB, Bader DM. The serosal mesothelium is a major source of smooth muscle cells of the gut vasculature. *Development* 2005; **132**:5317-5328.
18 Volz KS, Jacobs AH, Chen HI, *et al.* Pericytes are progenitors for coronary artery smooth muscle. *eLife* 2015; **4**:e10036.
19 Moore-Morris T, Guimaraes-Camboa N, Banerjee I, *et al.*

Resident fibroblast lineages mediate pressure overload-induced cardiac fibrosis. *J Clin Invest* 2014; **124**:2921-2934.
20 Chen Q, Zhang H, Liu Y, *et al.* Endothelial cells are progenitors of cardiac pericytes and vascular smooth muscle cells. *Nat Commun* 2016; **7**:12422.
21 Ali SR, Ranjbarvaziri S, Talkhabi M, *et al.* Developmental heterogeneity of cardiac fibroblasts does not predict pathological proliferation and activation. *Circ Res* 2014; **115**:625-635.
22 Zeisberg EM, Tarnavski O, Zeisberg M, *et al.* Endothelial-to-mesenchymal transition contributes to cardiac fibrosis. *Nat Med* 2007; **13**:952-961.
23 Mollmann H, Nef HM, Kostin S, *et al.* Bone marrow-derived cells contribute to infarct remodelling. *Cardiovasc Res* 2006; **71**:661-671.
24 van Amerongen MJ, Bou-Gharios G, Popa E, *et al.* Bone marrow-derived myofibroblasts contribute functionally to scar formation after myocardial infarction. *J Pathol* 2008; **214**:377-386.
25 Widyantoro B, Emoto N, Nakayama K, *et al.* Endothelial cell-derived endothelin-1 promotes cardiac fibrosis in diabetic hearts through stimulation of endothelial-to-mesenchymal transition. *Circulation* 2010; **121**:2407-2418.
26 Xu J, Lin SC, Chen J, *et al.* CCR2 mediates the uptake of bone marrow-derived fibroblast precursors in angiotensin II-induced cardiac fibrosis. *Am J Physiol Heart Circ Physiol* 2011; **301**:H538-547.
27 von Gise A, Pu WT. Endocardial and epicardial epithelial to mesenchymal transitions in heart development and disease. *Circ Res* 2012; **110**:1628-1645.
28 Friehs I, Illigens B, Melnychenko I, Zhong-Hu T, Zeisberg E, Del Nido PJ. An animal model of endocardial fibroelastosis. *J Surg Res* 2013; **182**:94-100.
29 Asfour B, Hare JM, Kohl T, *et al.* A simple new model of physiologically working heterotopic rat heart transplantation provides hemodynamic performance equivalent to that of an orthotopic heart. *J Heart Lung Transplant* 1999; **18**:927-936.
30 Kong P, Christia P, Saxena A, Su Y, Frangogiannis NG. Lack of specificity of fibroblast-specific protein 1 in cardiac remodeling and fibrosis. *Am J Physiol Heart Circ Physiol* 2013; **305**:H1363-H1372.
31 Zhang H, Pu W, Tian X, *et al.* Genetic lineage tracing identifies endocardial origin of liver vasculature. *Nat Genet* 2016; **48**:537-543.
32 Zhang H, Pu W, Li G, *et al.* Endocardium minimally contributes to coronary endothelium in the embryonic ventricular free walls. *Circ Res* 2016; **118**:1880-1893.
33 Madisen L, Zwingman TA, Sunkin SM, *et al.* A robust and high-throughput Cre reporting and characterization system for the whole mouse brain. *Nat Neurosci* 2010; **13**:133-140.
34 Zhang H, Pu W, Liu Q, *et al.* Endocardium contributes to cardiac fat. *Circ Res* 2016; **118**:254-265.
35 Akiyama H, Chaboissier MC, Behringer RR, *et al.* Essential role of Sox9 in the pathway that controls formation of cardiac valves and septa. *Proc Natl Acad Sci USA* 2004; **101**:6502-6507.
36 Garside VC, Cullum R, Alder O, *et al.* SOX9 modulates the expression of key transcription factors required for heart valve development. *Development* 2015; **142**:4340-4350.
37 Smith CL, Baek ST, Sung CY, Tallquist MD. Epicardial-derived cell epithelial-to-mesenchymal transition and fate specification require PDGF receptor signaling. *Circ Res* 2011; **108**:e15-26.
38 Ranger AM, Grusby MJ, Hodge MR, *et al.* The transcription factor NF-ATc is essential for cardiac valve formation. *Nature* 1998; **392**:186-190.
39 de la Pompa JL, Timmerman LA, Takimoto H, *et al.* Role of the NF-ATc transcription factor in morphogenesis of cardiac valves and septum. *Nature* 1998; **392**:182-186.
40 Chang CP, Neilson JR, Bayle JH, *et al.* A field of myocardial-endocardial NFAT signaling underlies heart valve morphogenesis. *Cell* 2004; **118**:649-663.
41 Acharya A, Baek ST, Huang G, *et al.* The bHLH transcription factor Tcf21 is required for lineage-specific EMT of cardiac fibroblast progenitors. *Development* 2012; **139**:2139-2149.
42 Lijnen PJ, Petrov VV, Fagard RH. Induction of cardiac fibrosis by transforming growth factor-beta(1). *Mol Genet Metab* 2000; **71**:418-435.
43 Bujak M, Frangogiannis NG. The role of TGF-beta signaling in myocardial infarction and cardiac remodeling. *Cardiovasc Res* 2007; **74**:184-195.
44 Tomita H, Egashira K, Ohara Y, *et al.* Early induction of transforming growth factor-beta via angiotensin II type 1 receptors contributes to cardiac fibrosis induced by long-term blockade of nitric oxide synthesis in rats. *Hypertension* 1998; **32**:273-279.
45 Nakajima H, Nakajima HO, Salcher O, *et al.* Atrial but not ventricular fibrosis in mice expressing a mutant transforming growth factor-beta(1) transgene in the heart. *Circ Res* 2000; **86**:571-579.
46 Rosenkranz S, Flesch M, Amann K, *et al.* Alterations of beta-adrenergic signaling and cardiac hypertrophy in transgenic mice overexpressing TGF-beta(1). *Am J Physiol Heart Circ Physiol* 2002; **283**:H1253-1262.
47 Schultz Jel J, Witt SA, Glascock BJ, *et al.* TGF-beta1 mediates the hypertrophic cardiomyocyte growth induced by angiotensin II. *J Clin Invest* 2002; **109**:787-796.
48 Kuwahara F, Kai H, Tokuda K, *et al.* Transforming growth factor-beta function blocking prevents myocardial fibrosis and diastolic dysfunction in pressure-overloaded rats. *Circulation* 2002; **106**:130-135.
49 Zeisberg M, Yang C, Martino M, *et al.* Fibroblasts derive from hepatocytes in liver fibrosis via epithelial to mesenchymal transition. *J Biol Chem* 2007; **282**:23337-23347.
50 Ueha S, Shand FH, Matsushima K. Cellular and molecular mechanisms of chronic inflammation-associated organ fibrosis. *Front Immunol* 2012; **3**:71.
51 Neustein HB, Lurie PR, Fugita M. Endocardial fibroelastosis found on transvascular endomyocardial biospsy in children. *Arch Pathol Lab Med* 1979; **103**:214-219.
52 Kretzschmar K, Watt FM. Lineage tracing. *Cell* 2012; **148**:33-45.
53 Nagy A. Cre recombinase: the universal reagent for genome tailoring. *Genesis* 2000; **26**:99-109.
54 Tian X, Pu WT, Zhou B. Cellular origin and developmental program of coronary angiogenesis. *Circ Res* 2015; **116**:515-530.
55 Zhang H, von Gise A, Liu Q, *et al.* Yap1 is required for endothelial to mesenchymal transition of the atrioventricular cush-

ion. *J Biol Chem* 2014; **289**:18681-18692.
56 Moore-Morris T, Cattaneo P, Puceat M, Evans SM. Origins of cardiac fibroblasts. *J Mol Cell Cardiol* 2016; **91**:1-5.
57 Zeisberg EM, Kalluri R. Origins of cardiac fibroblasts. *Circ Res* 2010; **107**:1304-1312.
58 Lane EB, Hogan BL, Kurkinen M, Garrels JI. Co-expression of vimentin and cytokeratins in parietal endoderm cells of early mouse embryo. *Nature* 1983; **303**:701-704.
59 Afonso PV, McCann CP, Kapnick SM, Parent CA. Discoidin domain receptor 2 regulates neutrophil chemotaxis in 3D collagen matrices. *Blood* 2013; **121**:1644-1650.
60 Hou G, Wang D, Bendeck MP. Deletion of discoidin domain receptor 2 does not affect smooth muscle cell adhesion, migration, or proliferation in response to type I collagen. *Cardiovasc Pathol* 2012; **21**:214-218.
61 Kaur H, Takefuji M, Ngai CY, *et al.* Targeted ablation of periostin-expressing activated fibroblasts prevents adverse cardiac remodeling in mice. *Circ Res* 2016; **118**:1906-1917.
62 Weber KT. Monitoring tissue repair and fibrosis from a distance. *Circulation* 1997; **96**:2488-2492.
63 Chong JJ, Chandrakanthan V, Xaymardan M, *et al.* Adult cardiac-resident MSC-like stem cells with a proepicardial origin. *Cell Stem Cell* 2011; **9**:527-540.
64 Lavine KJ, Yu K, White AC, *et al.* Endocardial and epicardial derived FGF signals regulate myocardial proliferation and differentiation *in vivo*. *Dev Cell* 2005; **8**:85-95.
65 Lavine KJ, White AC, Park C, *et al.* Fibroblast growth factor signals regulate a wave of Hedgehog activation that is essential for coronary vascular development. *Genes Dev* 2006; **20**:1651-1666.
66 Lavine KJ, Kovacs A, Ornitz DM. Hedgehog signaling is critical for maintenance of the adult coronary vasculature in mice. *J Clin Invest* 2008; **118**:2404-2414.
67 de la Pompa JL, Epstein JA. Coordinating tissue interactions: Notch signaling in cardiac development and disease. *Dev Cell* 2012; **22**:244-254.
68 Luna-Zurita L, Prados B, Grego-Bessa J, *et al.* Integration of a Notch-dependent mesenchymal gene program and Bmp2-driven cell invasiveness regulates murine cardiac valve formation. *J Clin Invest* 2010; **120**:3493-3507.
69 Zhang H, Pu W, Tian X, *et al.* Genetic lineage tracing identifies endocardial origin of liver vasculature. *Nat Genet* 2016; **48**:537-543.
70 Wang Y, Nakayama M, Pitulescu ME, *et al.* Ephrin-B2 controls VEGF-induced angiogenesis and lymphangiogenesis. *Nature* 2010; **465**:483-486.
71 Xu Z, Wang W, Jiang K, *et al.* Embryonic attenuated Wnt/beta-catenin signaling defines niche location and long-term stem cell fate in hair follicle. *eLife* 2015; **4**:e10567.
72 Friehs I, del Nido PJ. Increased susceptibility of hypertrophied hearts to ischemic injury. *Ann Thorac Surgery* 2003; **75**:S678-684.
73 Yu W, Huang X, Tian X, *et al.* GATA4 regulates Fgf16 to promote heart repair after injury. *Development* 2016; **143**:936-949.

(**Supplementary information** is linked to the online version of the paper on the *Cell Research* website.)